Molecular Therapy
Nucleic Acids
Original Article

The circular RNA Ataxia Telangiectasia Mutated regulates oxidative stress in smooth muscle cells in expanding abdominal aortic aneurysms

Francesca Fasolo,[1,2] Greg Winski,[3] Zhaolong Li,[1,2] Zhiyan Wu,[1,2,4] Hanna Winter,[1,2] Julia Ritzer,[1] Nadiya Glukha,[1] Joy Roy,[5,6] Rebecka Hultgren,[5,6] Jessica Pauli,[1,2] Albert Busch,[1,7] Nadja Sachs,[1] Christoph Knappich,[1] Hans-Henning Eckstein,[1] Reinier A. Boon,[8,9,10,11] Valentina Paloschi,[1,2] and Lars Maegdefessel[1,2,3]

[1]Department for Vascular and Endovascular Surgery, Klinikum rechts der Isar, Technical University Munich, 81675 Munich, Germany; [2]German Center for Cardiovascular Research (DZHK), Partner Site Munich Heart Alliance, 10785 Berlin, Germany; [3]Department of Medicine, Karolinska Institutet, 17177 Stockholm, Sweden; [4]Department of Vascular Surgery, Beijing Hospital, National Center of Gerontology and Institute of Geriatric Medicine, Chinese Academy of Medical Science, Beijing 100730, P.R. China; [5]Department of Molecular Medicine and Surgery, Karolinska Institutet, 17176 Stockholm, Sweden; [6]Department of Vascular Surgery, Karolinska University Hospital, 17176 Stockholm, Sweden; [7]Division of Vascular and Endovascular Surgery, Department of Visceral, Thoracic and Vascular Surgery, Medical Faculty, Carl Gustav Carus and University Hospital Carl Gustav Carus Dresden, Technische Universität Dresden, 01307 Dresden, Germany; [8]German Center for Cardiovascular Research DZHK 10785 Berlin, Partner Site Frankfurt Rhine-Main, Frankfurt am Main, Germany; [9]Institute of Cardiovascular Regeneration, Goethe University, 60590 Frankfurt am Main, Germany; [10]Amsterdam UMC Location Vrije Universiteit Amsterdam, Physiology, 1081 Amsterdam, the Netherlands; [11]Amsterdam Cardiovascular Sciences, Microcirculation, 1081 Amsterdam, the Netherlands

An abdominal aortic aneurysm (AAA) is a pathological widening of the aortic wall characterized by loss of smooth muscle cells (SMCs), extracellular matrix degradation, and local inflammation. This condition is often asymptomatic until rupture occurs, leading to high morbidity and mortality rates. Diagnosis is mostly accidental and the only currently available treatment option remains surgical intervention. Circular RNAs (circRNAs) represent a novel class of regulatory non-coding RNAs that originate from backsplicing. Their highly stable loop structure, combined with a remarkable enrichment in body fluids, make circRNAs promising disease biomarkers. We investigated the contribution of circRNAs to AAA pathogenesis and their potential application to improve AAA diagnostics. Gene expression analysis revealed the presence of deregulated circular transcripts stemming from AAA-relevant gene *loci*. Among these, the circRNA to the Ataxia Telangiectasia Mutated gene (c*ATM*) was upregulated in human AAA specimens, in AAA-derived SMCs, and serum samples collected from aneurysm patients. In primary aortic SMCs, c*ATM* increased upon angiotensin II and doxorubicin stimulation, while its silencing triggered apoptosis. Higher c*ATM* levels made AAA-derived SMCs less vulnerable to oxidative stress, compared with control SMCs. These data suggest that c*ATM* contributes to elicit an adaptive oxidative-stress response in SMCs and provides a reliable AAA disease signature.

INTRODUCTION

Abdominal aortic aneurysms (AAAs) are defined as localized pathological widening of the aortic diameter to more than 1.5 times its normal size.[1] Aortic aneurysms primarily affect the infrarenal aorta and are more prevalent among men over 65 years. Besides gender and age, risk factors include tobacco use and positive family history, suggesting a genetic association. On the molecular level, extensive loss of smooth muscle cells (SMCs) has been shown to be accompanied by metalloproteinase-mediated extracellular matrix degradation and local inflammation.[2] By further triggering metalloproteinase activity and SMC apoptosis, oxidative stress exacerbates the pathophysiology of inflammation, which may ultimately lead to thrombus formation.[3] Vessel dilation is often progressive, and AAAs remain mostly asymptomatic unless an acute rupture of the aortic wall occurs, accompanied by high mortality rates.[4] To date, established AAA prognostic indicators are still missing, making repeat imaging to monitor AAA expansion necessary. Furthermore, due to the lack of effective pharmacological treatments, the only available therapy is surgical intervention, either via an endovascular stenting approach or open repair (OR). The critical threshold for intervention is reached when the aortic diameter is found to be greater than 5.5 cm.[5] Identifying alternative, less-invasive therapeutic strategies relies on a deeper comprehension of the molecular mechanisms underlying AAA development and progression.

In the past decade, circRNAs have received increasing attention as a novel class of functional RNA molecules regulating biological processes' physiological and pathological aspects. CircRNAs are

Received 16 November 2022; accepted 14 August 2023;
https://doi.org/10.1016/j.omtn.2023.08.017.

Correspondence: Francesca Fasolo, Department for Vascular and Endovascular Surgery, Klinikum rechts der Isar, Technical University Munich, 81675 Munich, Germany.
E-mail: francesca.fasolo@tum.de

covalently closed RNA loops generated from backsplicing events in which a downstream 5' splice site (ss) is joined and ligated with an upstream 3′ ss.[6] They can be transcribed from either strand of exons (exonic circRNAs—the most abundant class) or introns (intronic circRNAs) of host genes. Circularization is often triggered by the presence of repetitive elements in backsplicing junction-flanking introns.[7] Although poorly expressed, their class-specific structural features confer higher stability than messenger RNAs (mRNAs), as the lack of a free -OH end makes them highly resistant to RNAseR degradation.[8,9] According to their subcellular localization, circRNAs contribute to the regulation of gene expression through multiple mechanisms. They participate in splicing, may act as miRNA or protein "sponges," and can interfere with the pre-mRNA processing machinery.[10] CircRNAs can be secreted in body fluids, including saliva and serum, making them ideal candidate biomarkers in clinical practice.[11]

In the context of cardiovascular disease (CVD), circular *ANRIL* (circ*ANRIL*) was the first circRNA to be associated to the molecular regulatory mechanisms at the basis of CVD risk phenotype at the cyclin-dependent kinase inhibitor 2A/B (*CDKN2A/B*) *locus*.[12,13] As of now, many circRNAs have been shown to significantly contribute to CVD pathophysiology.[14,15] The SMC-enriched circRNA circChordc1, for example, protects from AAA pathology by promoting SMC contractility and improving their survival.[16] cZNF292 contributes to the maintenance of the structural integrity of the aortic endothelium by regulating flow responses in endothelial cells (ECs).[17]

For this current study, we profiled differentially expressed circRNAs in AAAs *vs.* non-AAA human tissue specimens. Next, we investigated the role of the most promising candidates in AAA pathogenesis and progression and finally explored their potential application as a diagnostic AAA biomarker.

RESULTS

CircRNA profiling in human AAA disease

To evaluate the role of circRNAs in human AAA disease pathogenesis and disease progression, we performed a microarray analysis on a cohort of 17 human tissue specimens, including 6 non-AAA controls (CTRL, obtained from organ transplant surgery) and 11 AAA aortas collected from elective (e) OR surgery. The employed array chips (Arraystar, no. AS-S-CR-H-V2.0) cover all known annotated human circRNAs (13.617 in total), with array probes targeting circRNA-specific junctions. We discovered that a considerable amount of circRNA transcripts were significantly up- (40) or downregulated (51) in diseased tissue (Figure 1A; Table S1). Most deregulated targets in our dataset originated from circularization of one or multiple mRNA exons (exonic circRNA, Figures 1B and S1A). Exonic circRNAs have previously been shown to affect host gene expression by contributing to regulate most steps of RNA life, both in the nuclear (splicing and transcription) and in the cytosolic compartment (translation, stability, and degradation).[18] Among deregulated circRNA-cognate mRNAs, gene ontologies (GO) such as regulation of transcription and SMCs proliferation, which are well known established mechanistic drivers in AAA development, were found to be significantly enriched (Figure S1B). In light of this, in combination with p value and fold enrichment of differentially expressed circRNAs, as a main criterion to shortlist candidates for validation experiments, we prioritized targets transcribed from genes contributing to cellular processes of established relevance in AAA pathophysiology. circRNAs chosen for a first round of validation (12) are highlighted in yellow in Table S1.

To prove circularity of selected circRNAs, PCR with divergent primers was carried out in RNAseR-treated samples, and specificity of the resulting amplicons was checked by Sanger sequencing. Six out of 12 backsplicing junctions were successfully amplified and submitted for downstream analysis (Figure S2A). These corresponded to hsa_circ_0005660 (c*NFIX*), hsa_circ_0003641 (c*ATM*), hsa_circ0042103 (c*MYOCD*), hsa_circ003218 (c*BMPR2*), hsa_circ0004771 (c*NRIP1*), and hsa_circ0005615 (c*NFATC3*). Resistance to RNAseR digestion was assessed via comparison with a linear mRNA (*ACTA2*) in both eAAA tissue (Figure S2B) and human aortic SMCs (hAoSMCs) (Figure S2C), where all six circRNAs were successfully detected. Furthermore, subcellular localization of both circular and linear variants was profiled in hAoSMCs (Figure S2D). Circular variants were predominantly detected in the cytosolic compartment, even though considerable amounts were also present in the nucleus (except for c*NRIP*, for which this trend was reverted). Of note, most of the host genes of validated circular junctions encode for transcription factors (kinases) (Figure S3). Validation by qPCR of array results with respective primers was carried out, with a statistically significant result being observed for 3/6 circRNA targets (Figures 1C, S4A, and S4B). Deregulation trends of cognate mRNAs mirrored the ones detected for circRNAs (except for *NFIX*, Figure S4C).

c*ATM* is increased in human eAAAs, and its inhibition triggers *ATM* mRNA expression and apoptosis in AoSMCs

Inflammatory mediators and radical oxygen species (ROS), released by infiltrating immune cells, contribute to oxidative stress by inducing DNA damage, which in turn triggers apoptotic cell death within the AAA micromilieu. Among the top upregulated circRNAs, a four-exon circRNA spliced from the *ATM locus* caught our attention. Circular *ATM* (c*ATM*) deregulation trend was further confirmed in a separate AAA patient cohort (Figure S5A). Its expression was not restricted to the abdominal aorta, but could be also detected in human thoracic aorta specimens, in the carotid artery, as well as in the peripheral vasculature (Figure S5B). Besides multiple circular isoforms, all lacking coding potential (http://reprod.njmu.edu.cn/cgi-bin/circrnadb/circRNADb, with c*ATM alias* being *hsa_circ_12999*), *ATM* harbors 67 exons and 30 protein-coding transcript variants (https://www.ncbi.nlm.nih.gov), encoding for a ubiquitously expressed nuclear protein sensing double-strand break (DSB), while coordinating DNA damage response (DDR). Activated by autophosphorylation, ATM phosphorylates downstream p53, responsible for the initiation of the apoptotic cascade. According to the extent of the damage, apoptotic or survival gene programs are induced. However, the exact molecular dynamics responsible for cell fate decision

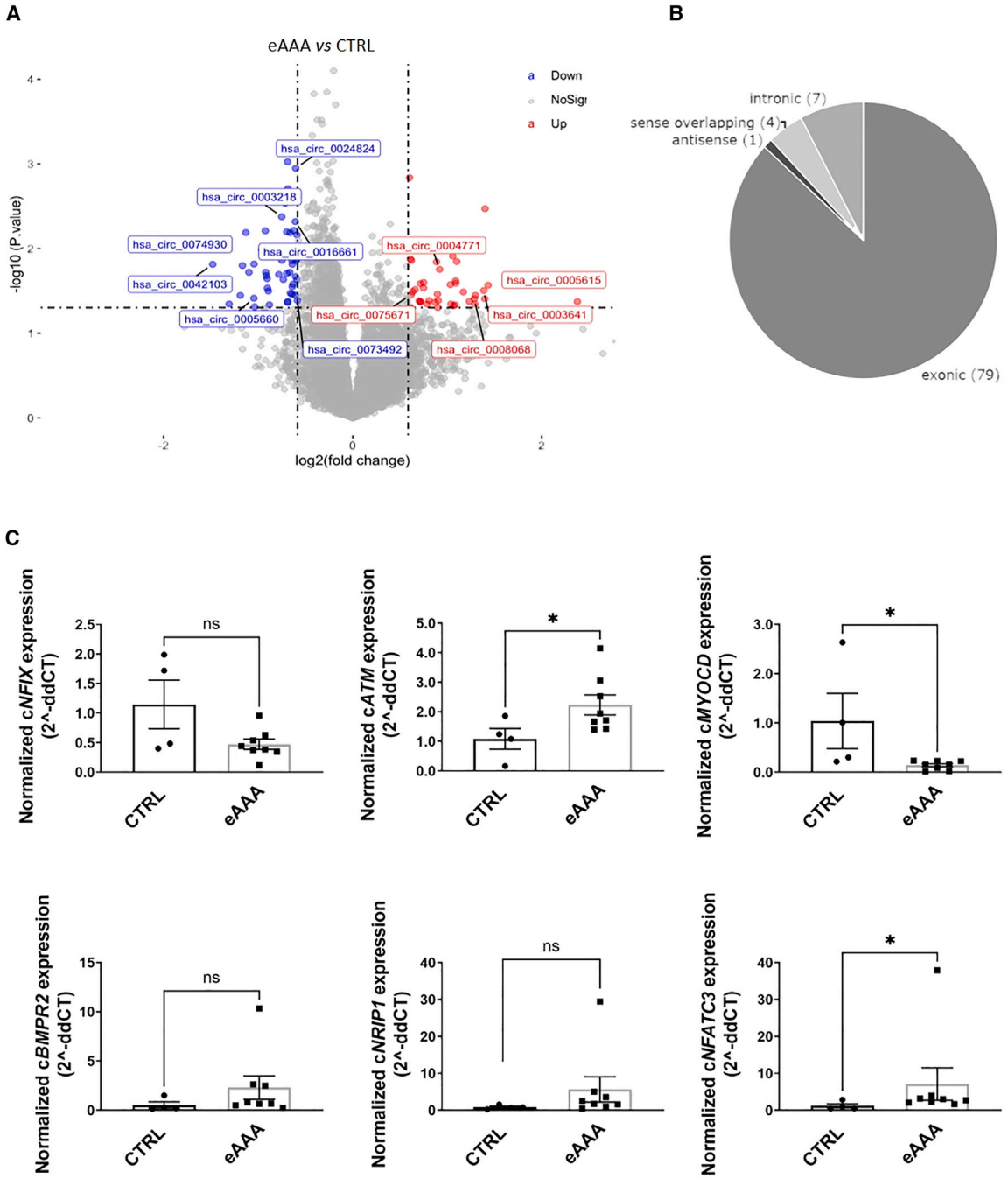

Figure 1. Circular RNAs are deregulated in human abdominal aortic aneurysm

(A) Volcano plot depicting downregulated (51, blue) and upregulated (40, red). Circular RNAs (circRNAs) in human elective human abdominal aortic aneurysm (eAAA, n = 11) *vs.* control (CTRL, n = 6) aorta specimens, as resulted by array experiments. Log2 fold change and -log10 p value are plotted on the x and y axes, respectively. IDs of circRNAs meant for a first round of validation are highlighted. Statistics: unpaired t test; p values <0.05 are considered significant. (B) Pie chart illustrating the proportion of exonic (89.8%), intronic (5.7%), sense overlapping (3.4%), and antisense (1.1%) array-identified differentially expressed circRNAs. Absolute numbers are further indicated for each group. (C) Real-time quantitative PCR (qPCR) validation of hsa_circ_0005660 (c*NFIX*), hsa_circ_0003641 (c*ATM*), hsa_circ0042103 (c*MYOCD*), hsa_circ003218 (c*BMPR2*), hsa_circ0004771 (c*NRIP1*), and hsa_circ0005615 (c*NFATC3*) differential expression in human eAAA (N = 8) and CTRL (N = 4) aortas. 2^{-ddCT} was calculated by normalizing on *RPLPO*. Data are represented as mean ± SEM. Statistics: unpaired t test; p values <0.05 are considered significant. NS, not significant; eAAA, elective AAA.

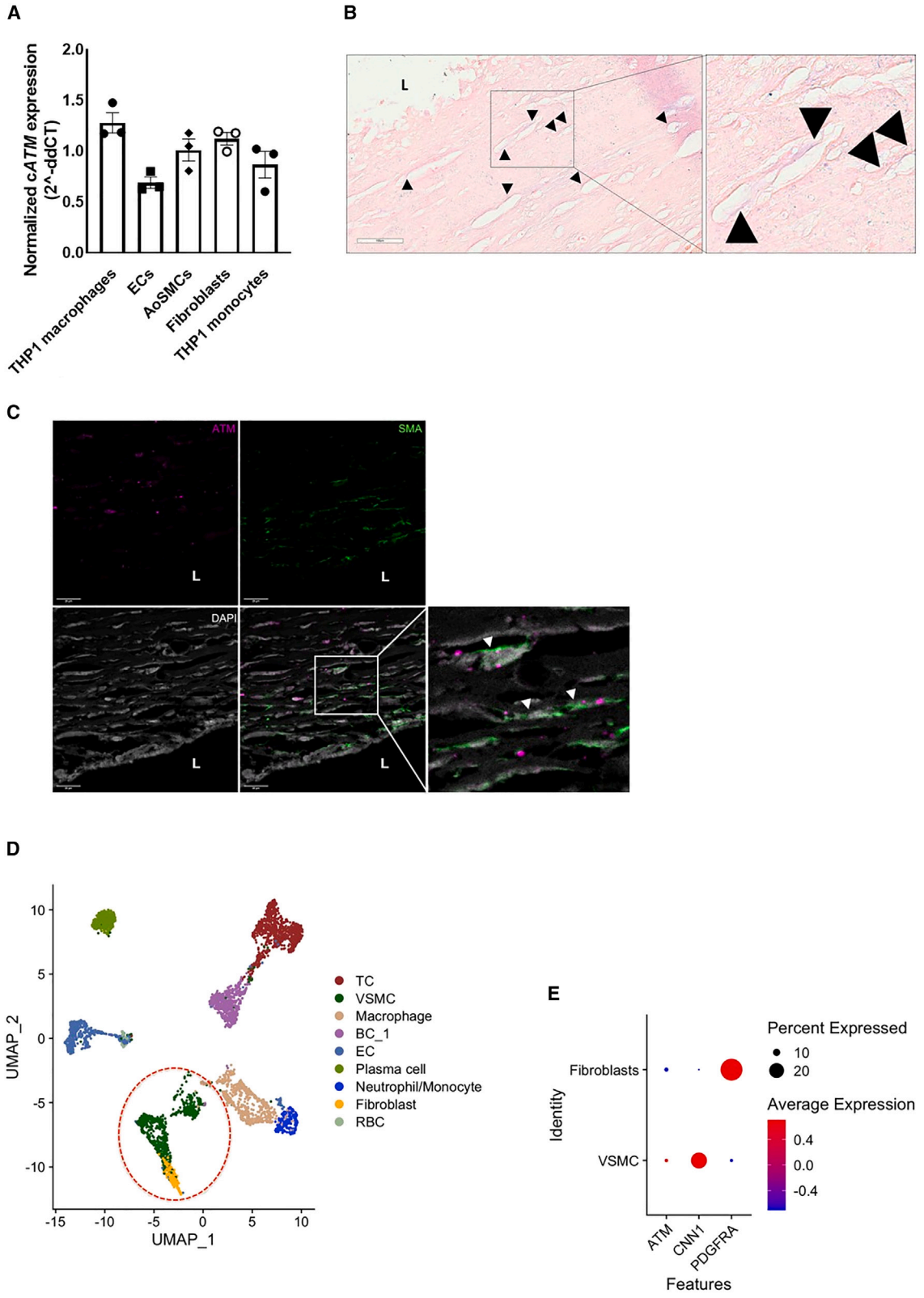

(legend on next page)

have yet to be elucidated. Comparison of CTRL *vs.* eAAA tissue revealed a trend towards increased c*ATM* and *ATM* levels (Figures 1A, 1C, and S4C), accompanied by downregulated ATM protein (Figure S6). We hypothesized that a regulatory loop involving c*ATM*/*ATM* mRNA/ATM protein could be crucial in stress response-related molecular dynamics in aneurysmal cells. c*ATM* profiling revealed similar expression levels in cultured structural vascular cells (ECs, AoSMCs, and fibroblasts), as well as THP1-derived monocytes and macrophages (Figure 2A). We chose to focus on AoSMCs as their loss is a main hallmark during AAA expansion.[19] Expression of c*ATM* was visualized in AAA sections by *in situ* hybridization (ISH) (Figure 2B). Smooth muscle cell α-actin (α-SMA) staining on consecutive slides corroborated c*ATM* presence in AoSMCs (Figures S7C and S7D), which was further indicated by ISH in cultured primary AoSMCs (Figure S7E). The circRNA is predominantly localized in the cytoplasm, even though a considerable amount appears in the nuclear compartment (Figures 2B and S2D). Immunohistochemistry (IHC) on human aneurysmal sections revealed ATM protein signal mostly in the *adventitia*, and to a lesser extent in the *media* (Figure S7A). Co-staining of ATM and α-SMA ensured ATM expression by AoSMCs (Figures 2C and S7B). Single-cell RNA sequencing (scRNA-seq) analysis carried out from four human AAA specimens confirmed ATM expression in aneurysmal vascular mural structural cells (Figures 2D, 2E, and S8).

We performed *in vitro* studies to further characterize *cATM* expression patterns in aortic disease. In line with results obtained from tissue analysis, *in vitro* AAA-mimicking angiotensin II (AngII) stimulation caused a remarkable c*ATM* increase (Figure 3A) in commercially available primary AoSMCs, derived from non-aneurysmal aortic donors. We then isolated primary AoSMCs from AAA patient biopsies and profiled c*ATM* in both AAA and non-AAA AoSMCs, which we refer to as CTRL AoSMCs. Interestingly, patient-derived cells displayed higher c*ATM* but lower *ATM* mRNA levels compared with CTRL ones (Figure 3B). To better elucidate the impact of c*ATM* in regulating host gene expression in AoSMCs, we conducted silencing experiments. We designed two alternative siRNAs targeting c*ATM* (Figure S9A), and observed that only sic*ATM*2 (and not sic*ATM*1) selectively targeted circular (Figure S9B, left and S9C) and not *ATM* mRNA (Figure S9B, right and S9C). Upon sic*ATM*2, in both AAA-derived and CTRL AoSMCs, *ATM* mRNA was significantly increased after 72 h (Figures 3C and 3D), although this did not affect ATM protein levels (Figure S9D). On the other hand, silencing of *ATM* affected exclusively the linear transcript and related protein (Figures S9B, right, S9C, and S9E). In CTRL AoSMCs, c*ATM* knockdown (KD) resulted in increased apoptosis, as measured by caspase-3/7 live-cell imaging (Figure 3E) and caspase-3/active caspase-3 western blotting (WB) signal (Figure 3F). This was further accompanied by an increase in p53 phosphorylation. Conversely, decreased expression of the survival protein BCL-2 could be observed (Figure 3F). *cATM* silencing further affected proliferation rates of CTRL AoSMCs, which was significantly decreased at 72 h post-transfection (Figure S10).

In summary, increased *cATM* expression detected in AAA tissue specimens was confirmed in AAA patient-derived cells. Opposing trends could be observed for *ATM* mRNA, which was upregulated in AAA tissue, but downregulated in patient cells. Moreover, in CTRL AoSMCS, c*ATM* depletion induced apoptosis and impaired their proliferation.

Higher c*ATM*-expressing AAA patient-derived AoSMCs are more resistant to oxidative stress

Once demonstrated that modulation of c*ATM* expression affected *ATM* mRNA levels and survival of AoSMCs, we hypothesized that its upregulation in patient-derived cells could be part of early stress-induced remodeling processes observed during AAA progression. Higher c*ATM* expression characterizing patient-derived cells seemed indeed beneficial rather than detrimental.

Delivery of exogenous c*ATM* via a plasmidic vector to CTRL AoSMCs (Figures S12A and S12B), almost counterintuitively, triggered AoSMCs death and negatively impacted proliferation (Figure S12C), with no effects observed in terms of *ATM* mRNA expression or p53 phosphorylation levels (Figures S12D and S12E). These results corroborated the hypothesis that higher levels of c*ATM* in disease might be an adaptive response rather than a causal event in AAAs. To further asses this, we compared the gene expression landscape of CTRL AoSMCs (coming from three different commercially available non-aneurysmal aortic donors) and five distinct AAA patient-derived AoSMCs. First, we confirmed that CTRL aorta- and aneurysm-derived cells presented significantly different gene expression profiles, giving rise to clearly separate clusters (Figure S13A). Next, we proved that the typical SMC gene signature was present in both AAA-derived and CTRL AoSMCs (Figure S13B). No substantial differences were detected in terms of expression of contractility markers, although *CCN1* and *MRTFA* were increased in CTRL cells. Conversely, AAA-derived cells displayed higher levels of synthetic

Figure 2. *ATM* and circular *ATM* are expressed in human AAA smooth muscle cells

(A) Expression of circular *ATM* (c*ATM*) in macrophages, mural vascular cells (endothelial cells [ECs]; aortic smooth muscle cells [AoSMCs]; and fibroblasts), and monocytes. 2^{-ddCT} was calculated by normalizing on *RPLPO*. (B) *In situ* hybridization (ISH) of c*ATM* (purple signal, black arrows). The c*ATM* probe was designed on the backsplicing junction. Scale bar, 100 μM. (C) Immunofluorescence on human AAA section showing co-localization of ATM (purple) and SMA (green) signal. Imaging was carried out with confocal microscopy. The zoomed area includes double-positive cells (white arrows). Scale bars, 20 μM. (D) Uniform Manifold Approximation and Projection (UMAP) plot shows the cell clusters identified by single-cell RNA sequencing (scRNA-seq) of n = 4 human AAA tissue specimens. Dotted red line highlights mural structural cell clusters (fibroblasts and SMCs). (E) Dot plot showing relative *ATM* expression in mural structural cell clusters (fibroblasts and SMCs) with respective expression profiles of one representative cluster's marker (*CNN1* and *PDGFRA*). Dot color represents the average expression level (blue, low; red, high) and dot size depicts the percentage of cells expressing the gene in a given cluster. L, lumen.

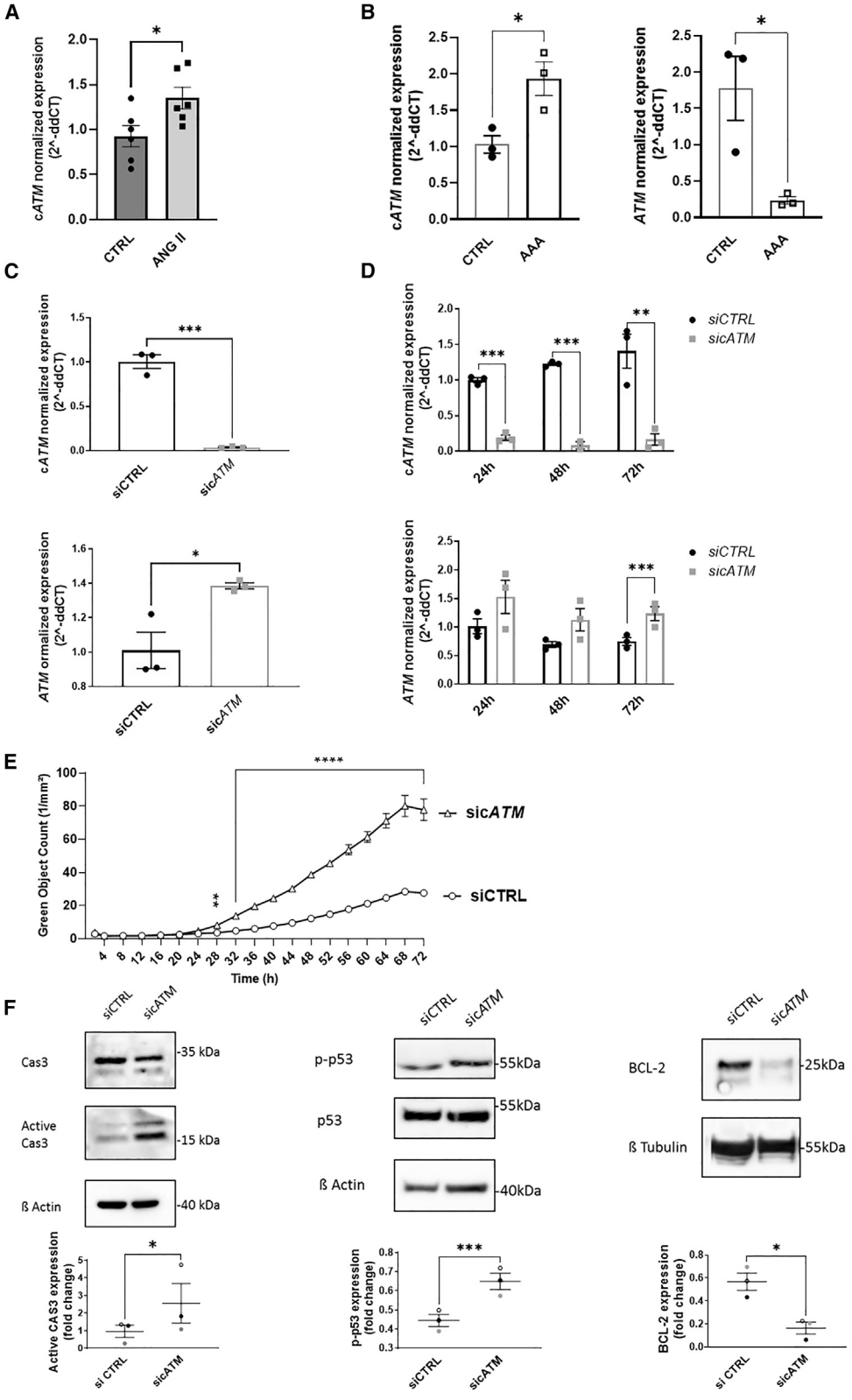

(legend on next page)

markers, such as collagen, FBN1, VIM, FN1, VCAN, and SERPINE1 (Figure S13B), highlighting active remodeling occurring. Significantly enriched Reactome pathways related to cell structure (extracellular matrix organization, degradation of the extracellular matrix) and signaling (GPCR ligand binding, signaling by GPCR, Table S2) were observed. Similar results were present in the GO term enrichment analysis: GO terms related to cell periphery and extracellular matrix were enriched in DEGs. Several GO terms associated with immune response and cellular motility were also enriched (including inflammatory response and cell migration, Table S3). Aiming at further corroborating a link between differential expression of c*ATM* (Figure 3B) and apoptosis (Figures 3E and 3F), we monitored gene expression of some of the main apoptosis (Figure 4A), proliferation, and cell-cycle markers (Figure 4B). Coherent with previous results, pro-apoptotic genes such as *CAS3* and *BOK* were downregulated in AAA-derived AoSMCs, while anti-apoptotic *BCL-2* was significantly upregulated (Figure 4A). Furthermore, a more vital proliferative *status* was supported by increased expression of proliferation and cell-cycle markers (Figure 4A). Targeted GO and pathway analysis further corroborated significant differences in the activation of apoptosis, DNA repair, and cell-cycle-related pathways (Figure 4D). Supporting a link between apoptosis/survival and ATM pathway, downstream ATM pathway genes *BID* and *BAX* were downregulated (Figure 4C) and, in line with this, default levels of phosphorylated ATM and p53 were lower in AAA-derived compared with CTRL cells, as revealed by WB (Figure 4E).

To explore the dynamics of c*ATM* regulation and its functional implications in a more endogenous-resembling setting, we mimicked the aneurysmal micromilieu by stimulating CTRL and AAA patient-derived AoSMCs with doxorubicin, which triggers oxidative stress (Figures 5 and S11). While c*ATM* levels in AAA-derived AoSMCs remained unaltered (Figure 5A, upper left), CTRL cells showed an augmented expression of the circRNA (Figure 4A, upper right), similar to that observed in AAA tissue specimens. Conversely, *ATM* mRNA was downregulated (Figure 5A, down) in both AAA-derived and CTRL cells. *ATM* and p53 phosphorylation was monitored as treatment control (Figure 5A, right). Of note, combined live-cell apoptotic assessment and WB pointed out lower apoptotic rates upon stress induction in AAA patient-derived AoSMCs compared with CTRL (Figure 5B). Taken together, these data suggest that higher c*ATM*-expressing AAA patient-derived AoSMCs are characterized by a greater resistance to oxidative stress, a more efficient DDR, and diminished apoptosis.

c*ATM* can be detected in serum of AAA patients and is elevated with disease

A crucial aspect for the application of circRNAs in clinical practice is their suitability to be employed as biomarkers, given their presence in body fluids (e.g., blood and saliva), as a results of sustained structural resistance to degradation. By taking advantage of serum samples collected from AAA patients undergoing elective surgery (eAAA) and age/sex-matched controls (CTRL) with peripheral artery disease (PAD), we compared c*ATM* expression between both groups. Circulating c*ATM* was significantly higher in AAA patients (Figure 6A), supporting that a certain range of c*ATM* expression might reflect the disease status. To further investigate the potential use of c*ATM* in AAA diagnostics, we compared its serum levels in elective *vs.* ruptured AAA patients. Although no statistically significant differences were found, a trend towards upregulation of c*ATM* was observed in the ruptured AAA group, suggesting that c*ATM* may be a negative prognostic indicator (Figure S14). Finally, we aimed at detecting ATM protein in blood. Interestingly, ATM levels were not significantly different between AAA and control (PAD) patients (Figure 6B), implying that only the circular isoform is potentially suited to diagnose patients with aortic aneurysms.

DISCUSSION

Abdominal aortic aneurysm is an asymptomatic condition accompanied by a high mortality rate related to its acute rupture risk. In Western countries, the annual incidence of new AAA diagnoses, which, despite screening programs, in some countries are mostly accidental, is approximately 0.4%–0.67%.[20–23] A clear disease etiology has yet to be established. However, the mechanisms at the basis of the development, dilation, and rupture of AAA have long been the object of scientific investigations. The anatomical characteristics and diameter of AAAs remain the only parameters to estimate individual risk of rupture and the timing of surgical intervention. As the natural history of AAA varies among patients, an accurate diagnosis would strongly benefit from specific molecular predictors, which, in combination with other known risk factors (e.g., age, male sex, smoking status, blood pressure, and dyslipidemia), could improve diagnosis and patient management.

Figure 3. Modulation of gene expression at *ATM locus* in AoSMCs

(A) Control (CTRL, n = 6) hAoSMCs were treated with 0.2 μM angiotensin II (AngII) for 24 h and *cATM* expression measured by qRT-PCR. Water served as control treatment. 2^{-ddCT} was calculated by normalizing on *RPLPO*. Statistics: unpaired t test; p values <0.05 are considered significant. Data are represented as mean ± SEM. (B) Comparison of c*ATM* (left) and *ATM* mRNA (right) expression in control donor (CTRL, n = 3) *vs.* AAA patient-derived hAoSMCs (AAA, n = 3) by qRT-PCR. 2^{-ddCT} was calculated by normalizing on *RPLPO*. Unpaired t test; p values <0.05 are considered significant. Data are represented as mean ± SEM. Statistics: (C) AAA (N = 3) and (D) CTRL (N = 3) hAoSMCs were transfected with 100 nM sic*ATM*2 and c*ATM* and *ATM* mRNA expression measured by qRT-PCR at different time points. 2^{-ddCT} was calculated by normalizing on *RPLPO*. Statistics: unpaired t test; p values <0.05 are considered significant. Data are represented as mean ± SEM. (E) KD effects on apoptosis were measured by live-cell imaging and quantification of fluorescent Cas3/7 (data are represented as mean ± SEM; statistics: multiple unpaired t test; p values <0.05 are considered significant). (F) Cas3/Active Cas3, p53/p-p53, and BCL-2 protein expression was further monitored as markers of cell apoptosis and survival, respectively. Quantification of immunoblots is reported in blots-flanking charts. Statistics: paired ratio t test; p values <0.05 are considered significant. Data are represented as mean ± SEM.

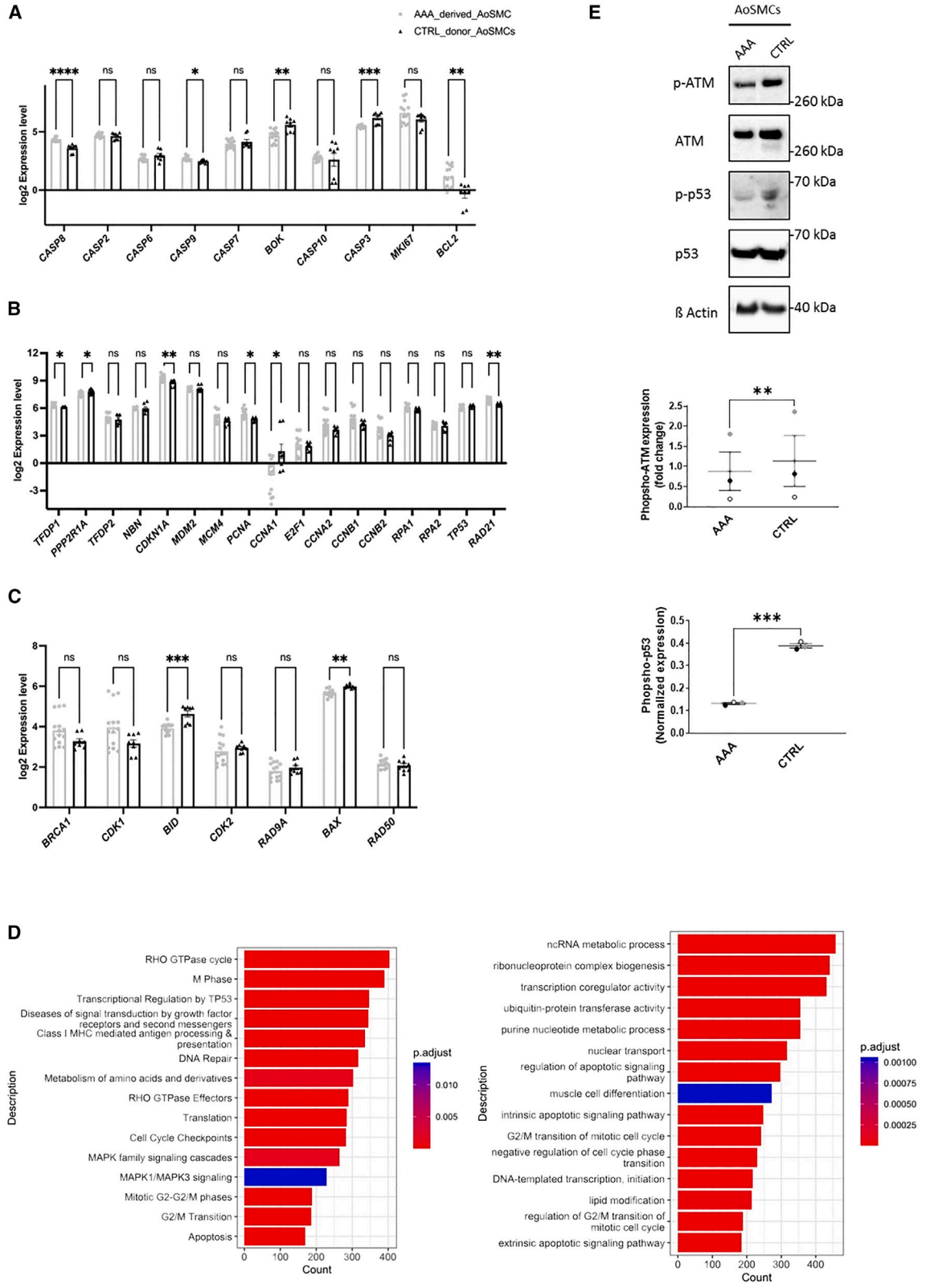

(legend on next page)

In the search for unexplored AAA gene expression signatures, we focused our attention on circRNAs. These are covalently closed RNA loops already described in the late 1970s in plant viroids.[24] Only more recently it was proven that they can exert critical regulatory functions in development and disease.[25,26] In addition to the regulation of gene expression at multiple levels and through multiple mechanisms, circRNAs are tissue specific and can be secreted into blood and saliva. Their circular structure, ensuring stability, makes them particularly suitable as biomarkers.[27] One criterion a candidate diagnostic biomarker has to meet is biological plausibility, establishing a cause-and-effect relationship between a natural factor and a particular disease.[28] Taking all of this into consideration, our study aimed at (1) profiling circRNAs expression in AAA *vs.* control human specimens, (2) selecting disease-relevant targets associated with functional phenotypes, and (3) addressing their clinical application as biomarkers.

To detect AAA-characterizing circRNAs, we took advantage of microarrays with backsplicing junction-mapping probes specific for all annotated circRNAs. Enzymatic (RNAseR) linear RNA removal was applied prior to hybridization to enrich, capture, and quantify circRNA targets with high sensitivity and specificity. Array-based quantification has the advantage of being less affected by the number of transcripts in individual samples, compared with RNA sequencing. However, a relevant drawback of RNAseR treatment is the potential loss of an undefined portion of circRNAs species, which may undergo degradation more efficiently.[29]

CircRNAs can be transcribed from different genomic regions and are accordingly distinguished into intergenic, intronic, or exonic. Exonic circRNAs share their exons with mRNAs and constitute the prevalent subgroup. In line with this, most differentially expressed circRNAs in our dataset had a linear mRNA counterpart. A growing body of evidence supports that non-coding circular transcripts affect gene expression at the *locus* of origin. Regulation may be achieved through the process of circularization itself[13] or, alternatively, circRNAs can be provided with specific functional features (reviewed in Yu et al.[30]). We prioritized validation of circRNA targets having a linear mRNA counterpart, whose deregulation affected cell proliferation, stress response, and apoptosis, which have a central role in AAA pathogenesis. mRNA expression of Ataxia Telangiectasia Mutated (*ATM*, a key regulator of the p53-mediated DDR) is increased in the tricuspid aortic valve and in the bicuspid aortic valve-associated thoracic aortic aneurysm (TAA) specimens and accompanied by a pro-proliferative state.[31] Different Malan syndrome-characterizing nuclear factor IX (*NFIX*) mutations have been previously associated with early-onset TAA development.[32] Myocardin (*MYOCD*) has been extensively acknowledged as an essential transcription factor for maintenance of the SMCs' contractility.[33] Bone morphogenetic protein (*BMP*) signaling is known to be tightly involved in pulmonary artery dilatation following pulmonary arterial hypertension.[34] Macrophage nuclear factor of activated T cell C3 (*NFATC3*) limits inflammation and foam cell formation.[35] The nuclear receptor interacting protein 1 (*NRIP1*) is a transcription factor modulating the transcriptional activity of the estrogen receptor.

Validation of array data in aortic tissue specimens confirmed differential expression of *cATM*, *cMYOCD*, and *cNFATC3*. In line with previous reports,[36] the identified deregulation trends of circRNAs and their respective linear counterparts were concordant. This would support the "microRNA sponge" functional model, where the upregulation of a given circRNA generates in turn, an increase of its cognate mRNA by sequestering and preventing specific microRNAs from silencing their targets. Interrogation of AAA scRNA-seq suggested that immune cells constitute the most represented clusters in our dataset. We reasoned that the identified deregulation trends in tissue would mostly mirror gene expression in these cell types. At aneurysmal sites, immune cells are indeed massively recruited and contribute to generate a stress-rich environment. ATM is one of the main PI3 kinases involved in sensing DSB and regulating the DDR. It is encoded by a multi-exonic mRNA (canonical form: 67 exons; 3,056 residues; 350 kDa) transcribed from the *ATM locus* at chr11, presenting about 30 annotated coding splicing variants.[37] ATM expression is particularly sustained in immune cells, ensuring an efficient coordination of the DDR. These are indeed particularly exposed to continuous genomic insults, due to abundant ROS production.[2] In the specific case of c*ATM/ATM*, both upregulated in diseased specimens, we propose that c*ATM* transcription could be induced by ATM protein depletion, as observed in AAA tissue, and that sponging of *ATM*-targeting miRNAs by c*ATM* would augment *ATM* mRNA available for translation. This represents a mechanism to promptly provide the cell with plenty of ready-to-translate mRNAs to sustain the synthesis of essential proteins, degraded as a result of metalloprotease activity, immune cell infiltration, and inflammation-induced oxidative stress. Supporting this mechanistic model, c*ATM* contains binding sites for *ATM*-targeting miR-567, miR-4677 5p, and miR-4778 5p. However, this remains to be further investigated with more immune cell-focused experiments. Instead, we chose to specifically focus our attention on AoSMCs, as the most affected cell population in AAA, with oxidative stress representing a major threat to their integrity during disease progression. We aimed at dissecting the effects of c*ATM*-mediated regulation of *ATM* expression and how this affects networks controlling cell fate. ATM, indeed, directs cells towards survival or programmed cell death, although the

Figure 4. Expression profile of apoptosis-, cell-cycle-, and ATM pathway-related gene-related genes in AAA patient-derived *vs.* CTRL AoSMCs

Differential expression of apoptosis-related (A), cell-cycle-related (B) and ATM pathway-related (C) genes in AAA patient-derived (gray) *vs*. CTRL (black) AoSMCs, as of RNA-seq. Log2 expression levels are plotted. Statistics: unpaired multiple t test; p values <0.05 are considered significant. Data are represented as mean ± SEM. (D) Targeted Reactome-based (top, https://reactome.org/) or gene ontology (GO)-based (bottom, https://geneontology.org/) gene set enrichment analysis (GSEA) was performed to determine whether sets of genes involved in pathways/GO-terms of interest (i.e., apoptosis, cell-cycle and DNA damage) tended to be significantly ($p < 0.05$) over-represented. (E) Western immunoblot comparing phosphorylation status of ATM pathway proteins (ATM and p53) in AAA patient- (left) and CTRL donor-derived AoSMCs (right).

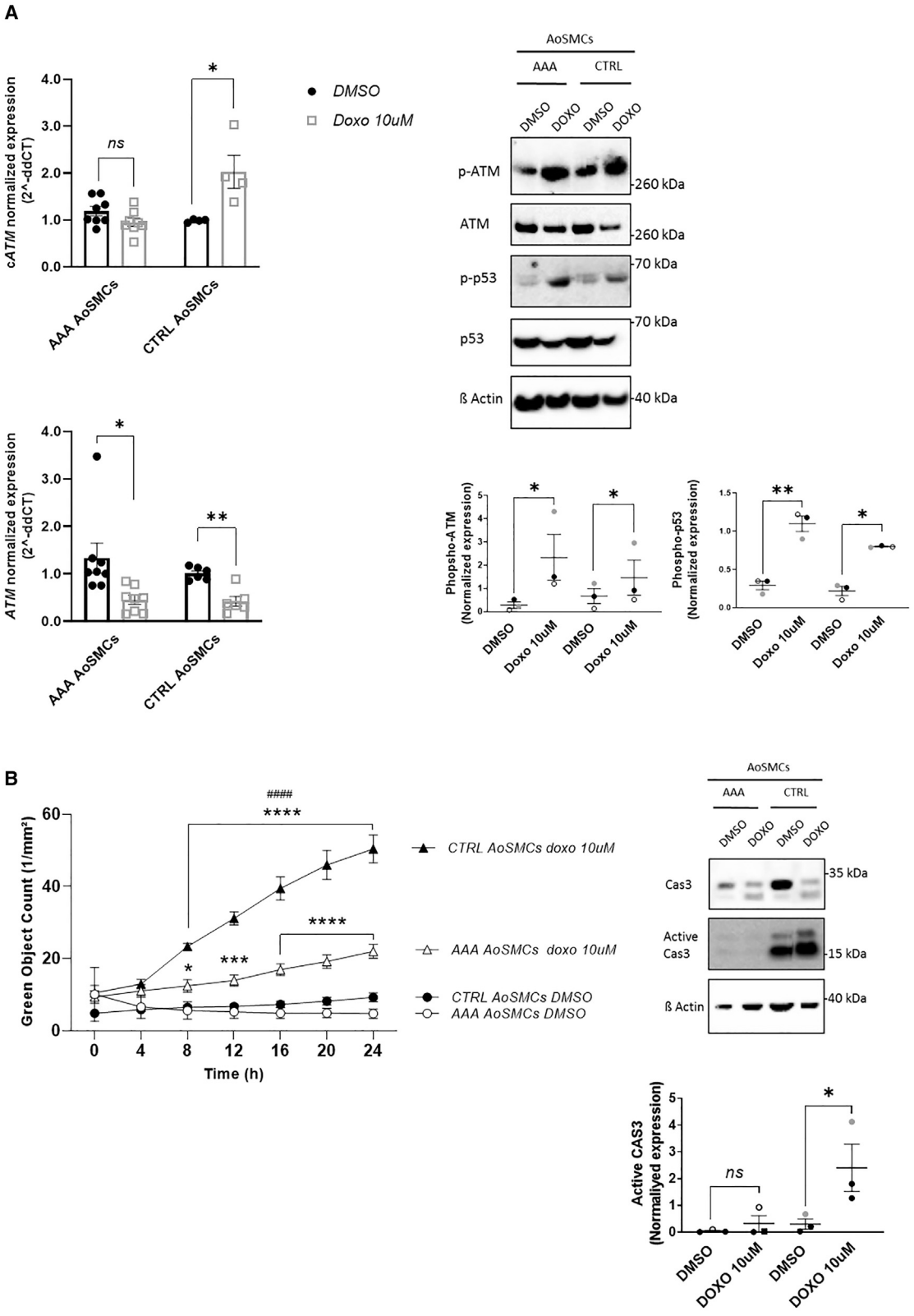

(legend on next page)

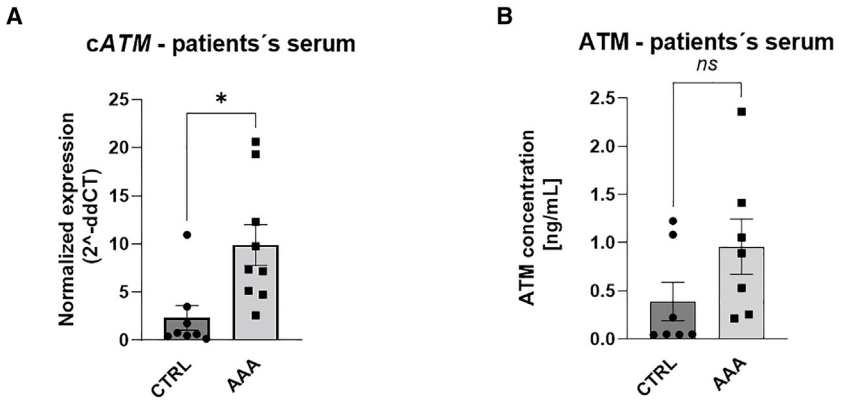

Figure 6. Circulating c*ATM* as AAA biomarker

(A) c*ATM* expression was monitored in serum samples collected from AAA (N = 9) and peripheral artery disease (PAD) (N = 8) patients. The latter were used as control group. 100 ng of an *in-vitro*-transcribed *GFP* RNA were spiked in into each sample and used as a reference to calculate 2^{-ddCT}. (B) Sandwich ELISA was performed to monitor the expression of ATM protein in patients' serum (7 PAD *vs*. 7 AAA). ATM concentration was calculated based on the standard curve. Statistics: unpaired t test; p values <0.05 are considered significant. Data are represented as mean ± SEM. (C) Proposed mechanism of c*ATM*-mediated regulation of *ATM* expression and its effects on survival/apoptosis in human AoSMCs.

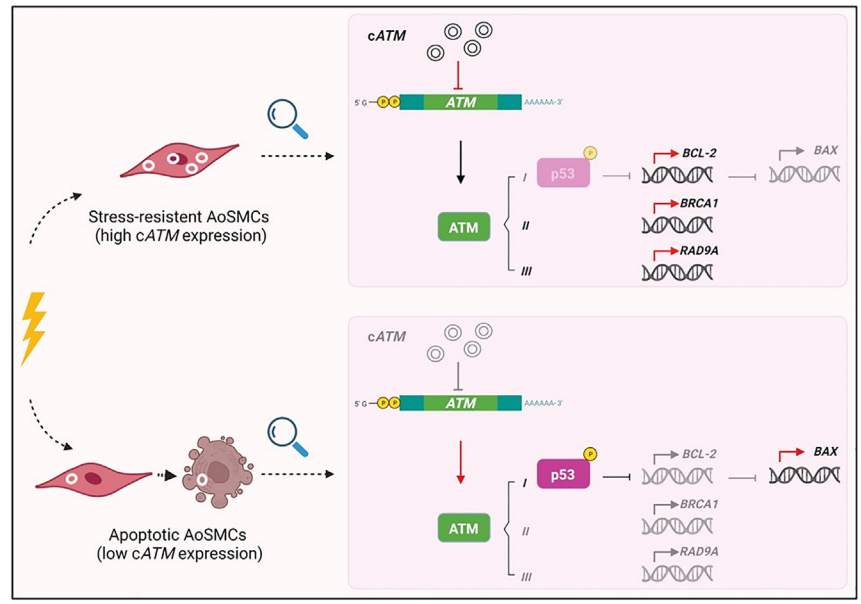

molecular mechanism underlying this decision-making is not clear. In the case of induced apoptosis, ATM, activated by autophosphorylation, can in turn phosphorylate downstream p53, responsible for the initiation of the apoptotic cascade. We discovered that c*ATM* was up-regulated in angiotensin II-treated CTRL AoSMCs (derived from non-aneurysmal aortas), and its expression levels in AAA patient-derived AoSMCs were significantly higher compared with CTRL ones. Contrary to what was observed in bulk tissue, linear *ATM* expression was depleted in AAA cells in comparison to CTRL cells.

In line with this, c*ATM* silencing resulted in higher levels of *ATM* in both CTRL and AAA patient-derived AoSMCs. This adds a further layer of complexity to data interpretation, implying that the grammar of *cATM* regulation in AoSMCs differs from the "miRNA sponge" model. Interestingly, c*ATM* deprivation in CTRL AoSMCs was associated with higher apoptosis and decreased proliferation rates. Even if disease-related, higher expression levels of c*ATM* in AAA seemed to thus be protective, rather than detrimental. This was further corroborated by (1) sequencing of CTRL and AAA-derived cells, which pointed out increased expression of survival genes and a more vital proliferation state of AAA-derived AoSMCs and (2) a higher tolerance of the latter to doxorubicin-induced oxidative stress.

Furthermore, we also recorded a global increase in default levels of phosphorylated p53 in CTRL cells, which could be further increased by knocking down c*ATM*. We propose that a negative endogenous c*ATM*/*ATM* loop contributes to regulate ATM pathway in AoSMCs, by tuning phosphorylation of p53 and, eventually, cell fate, similar to what was reported in a previous study.[38] The molecular dynamics at the basis of this phenotype unfortunately remain undefined, as our attempts to demonstrate a physical interaction between c*ATM* and p53 by RNA immunoprecipitation, and to link this to differential phosphorylation of the latter failed (data not shown). We cannot exclude that low c*ATM* expression and qPCR detection limits

Figure 5. Effects of doxorubicin-induced oxidative stress in AAA patient-derived *vs*. CTRL AoSMCs

(A) AAA patient- (left, n = 8) and control donor-derived AoSMCs (right, n = 6) were treated with 10 μM doxorubicin (doxo) or 0.001% DMSO for 24 h and c*ATM* (top) and *ATM* mRNA (bottom) expression measured by qRT-PCR (left). 2^{-ddCT} was calculated by normalizing on *RPLPO*. ATM, phospho-ATM, p53, and phospho-p53 protein levels were also compared by WB (right). Statistics for qPCR: unpaired t test; statistics for WB: paired ratio t test. In both: p values <0.05 are considered significant. Data are represented as mean ± SEM. (B) Treatment effects on apoptosis were measured by live quantification of fluorescent Cas3/7 and WB on Cas3/Active Cas3 protein. (*) Refers to comparison between treated/untreated CTRL or AAA-patient derived AoSMCs, (#) refers to comparison between treated CTRL *vs*. AAA patient derived SMCs. Multiple unpaired t test; p values <0.05 are considered significant. Data are represented as mean ± SEM.

could have contributed to the observed experimental output. However, in line with our findings, in their study on DDR in an inducible human neural stem cell line, Carlessi et al. showed that ATM protein depletion attenuates the ionizing radiation-induced DDR, as shown by reduced phosphorylation of the ATM target p53 and, in turn, the p53-dependent apoptotic response.[39]

When assessing the effects of c*ATM* overexpression, we were surprised to see that, similar to KD, forced induction resulted in increased apoptosis and limited proliferative rates. We are convinced that this attempt to model AAA via overexpression has its limitations, such as (1) the delivery through plasmidic vectors of a high number of target copies might not replicate increased endogenous expression and/or interfere with the proper subcellular localization, (2) the presence of inverted repeats could trigger double-stranded RNA-activated pathways mediating stress-induced apoptosis,[40,41] and (3) regulation of transcription at *ATM locus* can be unaffected by c*ATM* transient transfection. This is supported by the lack of effects on endogenous *ATM* mRNA expression following c*ATM* overexpression. We strongly believe that the administration of disease-mimicking stimuli, such as angiotensin II or doxorubicin, are more likely to resemble endogenous *cATM* expression and regulation. Furthermore, primary AoSMCs directly isolated from AAA patient biopsy are, in our opinion, the most suitable disease *in vitro* model to study endogenous regulatory mechanisms. The different AoSMCs utilized in our study (AAA patient-derived *vs.* non-dilated aorta donor [CTRL]) expressed different levels of c*ATM* and, accordingly, presented different phenotypic states of the diseased and non-diseased aorta. Even though sequencing was performed on CTRL and AAA-derived cells from different individuals, we found that the two groups form well-separated clusters, differing in the expression of stress response and apoptosis-related genes. Together with our functional experiments, this profiling further corroborated our hypothesis of having selected a population of "AAA-adapted" cells, with augmented resistance to stress. It is widely acknowledged that inflammatory mediators contribute to phenotypic remodeling and functional alterations in AoSMCs during AAA development (reviewed in Qian et al.[42]). We postulated that stress-triggered c*ATM* transcription could work as a signal for activating survival pathways (like *BCL-2*) by fine-tuning *ATM* expression levels. Although the molecular dynamics at the basis of c*ATM* transcription and the specific mechanism through which this circRNA inhibits the expression of its linear counterpart remain to be elucidated, our work shows that circRNA expression is crucial in determining and maintaining phenotypic variability among SMCs (Figure 6C).

The reason why we chose to evaluate more thoroughly c*ATM* (and not c*MYOC* or c*NFATC3*) was based on three main assessments. Firstly, its expression levels in the analyzed tissue cohort and in hAoSMCs were high enough to permit reliable and reproducible detection by qRT-PCR. Secondly, we valued the extreme importance of its linear counterpart *ATM* in the dynamics underlying cellular responses to oxidative stress, which represents a major cause of SMC death in AAA. Finally, based on our translational experience, a therapeutic manipulation of disease upregulated (rather than downregulated) targets, relying on silencing strategies (siRNAs or Gapmers), has less technical challenges and is more likely to be successful *in vitro* and *in vivo*, compared to overexpression, which requires the use of viral vectors. However, a noteworthy limitation of this study is the lack of *in vivo* experiments supporting our *in vitro* findings. In the perspective of predicting AAA prognosis, for example, *in vivo* c*ATM* KD would be a key experiment. Indeed, given the observed augmented SMC apoptosis upon silencing, this would allow monitoring whether c*ATM* depletion makes aneurysms more prone to rupture. The absence of annotated c*ATM* murine homologs prevented us from reproducing the disease-related patterns detected in human tissue, SMCs and serum in experimental AAA mouse models.

We eventually showed that *cATM* expression profiles could be exploited as a diagnostic tool accessible in circulating blood. Coherent with our previous findings, c*ATM* was indeed upregulated in serum samples collected from AAA patients. We presently lack diagnostic tools capable of predicting the rapidness of AAA growth, and the definition of further reliable criteria for stratification of patients, based on AAA rupture risk, would be highly desirable. It would be challenging to claim that a circRNA could be per se used as a biomarker in AAA screening, but we are confident in stating that, given their high stability and relatively low detection costs, circRNA could play an essential role in molecular AAA diagnostics in the near future. Although further research is still needed to assess its suitability in AAA diagnosis and prognosis, we propose assessing circRNA profiles as a valuable compliment to the current diagnostic gold standard of B-mode ultrasound imaging.

Conclusions

In summary, our work emphasizes the importance of investigating non-coding RNA-mediated gene expression regulation as a tool to improve our comprehension of AAA molecular dynamics. In particular, we were able to provide an example of a circRNA disease signature and propose c*ATM* transcription as part of an early stress response triggered by AAA-characteristic microenvironmental changes. By regulating gene expression at the *ATM locus* and contributing to the activation of survival pathways, c*ATM* upregulation functions as an "early warning signal" that promotes a switch towards stress-resistant SMC phenotypes.

MATERIALS AND METHODS

Human sample collection and storage

Human samples employed in this study were provided by the Munich Vascular Biobank and the Stockholm Aortic Aneurysm Biobank. AAA tissue specimens or blood were collected from patients who underwent elective surgical repair in both hospitals. Aortic fragments harvested in organ explant procedures or serum from patients with PAD were used as respective controls. Tissue specimens were put in RNA later for 24 h, and then snap frozen and stored at −80°C. All patients provided their written informed consent and in accordance with the Declaration of Helsinki. The studies were approved by the local ethics committees. All patient samples were matched

for age (average: 65.26 years) and sex (90% males). A detailed list of human samples used in this study is reported on Table S4.

CircRNA array experimental pipeline and analysis

For circRNA array experiments (Arraystar, Rockville, MD), AAA tissue specimens were collected from patients who underwent elective surgical repair (n = 11), while healthy aortic fragments were harvested from kidney transplant donors and used as controls (n = 6). Upon RNA extraction and quality control (QC), samples were treated with RNAseR (Epicentre, Teddington, UK), and reverse transcribed by using fluorescently labeled random primers. The resulting labeled cDNA was then purified and 1 μg was fragmented, heated, and subsequently hybridized with an 8 × 15k commercially available array chip displaying 13,617 human circRNAs (Arraystar, no. AS-S-CR-H-V2.0) for 17 h at 65°C in an Agilent Hybridization Oven. Array probes were designed on the backsplicing junction. After washing of slides, the arrays were scanned by using the Agilent Scanner G2505C. Agilent Feature Extraction software (v.11.0.1.1) was used to analyze acquired array images. Quantile normalization and subsequent data processing were performed using the R software limma package. The analysis did not return any differentially regulated circRNA after false discovery rate (FDR) correction. Therefore, significantly differentially expressed circRNAs between two groups were defined as having an absolute fold change >1.5 and $p < 0.05$. Based on these conditions, gene overexpression analysis of GO terms was performed, based on the categorization of their linear RNA counterparts by utilizing "Cluster Profiler" R function.

Primary cell culture of human aortic aneurysm SMCs

Written and informed consent was obtained from all patients, and protocols were approved by the local ethics committee. Human AAA specimens were harvested during surgical repair and stored in complete DMEM/F12 medium containing 5% FBS and 1% PBS (Millipore, Darmstadt, Germany). The tissue was placed in a sterile Petri dish and washed with PBS. *Adventitia*, neo-*intima*, and excessive calcification were removed, and the remaining tissue was cut into small pieces by using a sterile scalpel. Enzymatic digestion was carried out in complete DMEM/F12 medium implemented with 1.4 mg/mL collagenase A (Roche, Penzberg, Germany), for 4–6 h in a humidified incubator at 37°C and 5% CO_2. Cells were strained by using a 100 μm cell strainer to remove debris. After two washes, cells were resuspended in 7 mL complete DMEM/F12 medium and placed in culture in a small cell culture flask in a humidified incubator at 37°C and 5% CO_2. Medium was changed every other day. After 7 days, the medium was replaced with SMC Growth Medium (PeloBiotech, Planegg, Germany). Cells were used between passages 3 and 11. Primary AoSMCs from healthy donors (control AoSMCs, CTRL) were purchased from Cell Applications (no. 354-05a) and cultured in SMC growth medium, following the manufacturer's instructions. Cells were used between passages 5 and 7.

Validation of circular junctions

For circRNA analysis, RNAseR (Lucigen) was applied to extracted RNA at a concentration of 2 U/μg RNA for 15 min at 37°C, followed by enzyme inactivation for 20 min at 65°C and column-based purification (QIAGEN, no. 74204). First-strand cDNA synthesis was performed with the High-Capacity-RNA-to-cDNA Kit (Applied Biosystems, Waltham, MA) according to the manufacturer's instructions, starting from equal amounts of purified RNA. Divergent primers were designed to amplify the circular junction by taking advantage of the circInteractome tool (https://circinteractome.nia.nih.gov/). Oligonucleotide sequences and provider details are reported in Table S5. PCR products were visualized by using a FastGene UV Transilluminator (Nippon Genetics, Düren, Germany) and individual bands were gel-extracted (QIAGEN) and subsequently cloned into a TOPO TA Cloning Kit (Invitrogen) for Sanger sequencing (Eurofins Genomics, Ebersberg, Germany). Sequencing results are reported on Figure S15.

c*ATM* overexpression vector design and subcloning

c*ATM* overexpression vector design was carried out according to https://doi.org/10.1007/978-1-4939-7562-4_8. In particular, c*ATM* mature sequence (526 nts, https://circinteractome.nia.nih.gov/api/v2/circmature?circular_rna_query=hsa_circ_0003641) together with the adjacent ∼200 bp upstream and ∼200 bp downstream intronic fragments were flanked by inverted repeat-containing MLLT3/AF9 intron 4 (chr9:20,414,651-20,415,428, hg38), with the aim of triggering circularization. Gene synthesis (Eurofins) was carried out in pMS-RQ (SpcR/StrR) vector, and XhoI and EcoRV restriction sites were exploited for subcloning into pcDNA3.1-HisC. Positive clones were screened by colony PCR, re-amplified for MINI prep, and eventually Sanger sequenced. Details of c*ATM* overexpression vector sequence construction and sequence are reported in Figures S16–S18.

Silencing, transfection, and doxorubicin treatment of human aortic SMCs

CircRNA/mRNA silencing was performed by using Lipofectamine RNAiMAX (Thermo Fisher Scientific, Waltham, MA) reagent, according to the manufacturer's instructions. siRNAs targeting the backsplicing junction were designed with the help of the CircInteractome tool (https://circinteractome.nia.nih.gov/) and used at a final concentration of 100 nM for 48 or 72 h. A scrambled siRNA (Ambion) was employed as negative control. A complete list of siRNA sequences is reported in Table S7. For overexpression experiments in a 48-well format, 62.5 ng of c*ATM*/pcDNA3.1-HisC or empty vector were utilized, in combination with 0.125 μL of Lipofectamine 3000. Harvesting was performed at 48 h post-transfection. For doxorubicin treatment, 10 μM doxorubicin (Sigma, D1515) or 0.001% DMSO (Sigma, D8418) in cell medium was administered to cells for 24 h. Phosphorylation of p53 was used as treatment readout.

RNA isolation and gene expression analysis

Total RNA was isolated with a QIAzol-based (QIAGEN) RNA isolation protocol, by taking advantage of miRNeasy Mini (for tissue) or Micro (for cells) Kit (QIAGEN). RNA was quantified by NanoDrop (Wilmington, DE) and RNA quality was verified with Agilent 2100 Bioanalyzer (Agilent Technologies, Santa Clara, CA). DNAse (QIAGEN) was applied to avoid artifacts deriving from DNA

contamination. First-strand cDNA synthesis was performed with the High-Capacity-RNA-to-cDNA Kit (Applied Biosystems) according to the manufacturer's instructions, starting from equal amounts of purified RNA. Real-time quantitative PCR (qPCR) was performed on a QuantStudio3 Real-Time PCR System (Applied Biosystems) using Sybr-Green PCR Master Mix (Roche, Planegg, Germany) or TaqMan Fast Advanced Master Mix (Applied Biosystems). Oligonucleotide sequences/TaqMan assays used in this paper are listed in Table S5. Amplified transcripts were quantified by using the comparative Ct method and relative gene expression calculated by the method of ΔΔCt.[43]

Digital PCR

c*ATM* copy number was assessed by exploiting an absolute Q Digital-PCR (dPCR)-System (Applied Biosystems) in tissue from AAA patients undergoing OR surgeries. In particular, the cohort included specimens in which both the non-aneurysmal aortic neck (non-dilated control, n = 3) and the adjacent aneurysmal segment (dilated AAA, n = 3) were collected. RNA/cDNA (12.5 ng) was used as input for each dPCR reaction. Reactions were set up according to the manufacturer's instructions and performed in duplicate for c*ATM*. *RPLPO* copy number was also quantified in separate reactions and used as a reference in data analysis, which was carried out following Coulter's template.[44] In brief, based on the theoretical amount of RNA/cDNA used as input (12.5 ng) and the obtained number of *RPLPO* copies/reaction, the number of c*ATM* copies per ng input RNA was finally inferred. An Excel spreadsheet with calculations is provided as Table S6.

RNA isolation from serum

RNA was isolated from nine AAA and eight PAD patients' serum by using the miRNeasy Serum/Plasma Advanced Kit (QIAGEN), following the manufacturer's instructions, with some modifications. In brief, 1.25 μL of MS2 RNA (Roche) and 100 ng of IVT *GFP* RNA (as spike-in control) were combined with 500 μL of serum. After adding 240 μL of buffer RPL, samples were incubated at room temperature for 3 min. Buffer RPP (80 μL) was further added and incubated for 3 min. After centrifugation, the supernatant was mixed with 1 volume isopropanol and transferred to an RNeasy UCP MinElute column. RWT and RPE washings were eventually followed by RNA precipitation in 80% ethanol. Elution was carried out in 20 μL RNase-free water.

scRNA-seq

Human aneurysmal abdominal arteries were harvested during OR in the Department of Vascular and Endovascular Surgery at the Klinikum rechts der Isar of the Technical University Munich. After enzymatic digestion, tissue dissociation was performed using the Multi Tissue Dissociation Kit 2 (Miltenyi Biotech, 130-110-203), GentleMACS Dissociator (Miltenyi Biotech, 130-093-235), GentleMACS C tubes (Miltenyi Biotech, 130-096-334), and the 37C_Mulit_G program, all according to the manufacturer's instructions. The cell suspension was strained (70 and 40 μm) and Dead Cell Removal (Miltenyi Biotech, 130-090-101) using MS Columns (Miltenyi Biotech, 130-042-201) was performed. Cells were resuspended in PBS + 0.04% BSA. Cells were loaded into a 10x Genomics microfluidics Chip G and encapsulated with barcoded oligo-dT-containing gel beads by utilizing the 10x Genomics Chromium Controller. Gel beads-in-emulsion (GEM) clean-up, cDNA Amplification, and 3′ Gene Expression Dual Index Library Construction was performed according to the manufacturer's instructions (CG000315 Rev C). Sequencing was performed by taking advantage of an Illumina NovaSeq 6000 Sequencing system. Data relative to n = 4 AAA patient specimens (duplicates) were used to perform the downstream analysis. Raw data obtained from sequencing were demultiplexed according to the 10x Genomics pipeline by using Cell Ranger (v.3.1.0, v.5.0.0, and v.6.0.0) software (10x Genomics). A gene-barcode matrix was generated for each library, and cell barcodes and UMIs were corrected and filtered. Single-Cell Data Analysis R package Seurat (v.4.1.1)[45,46] was used for the analysis in RStudio (v.1.4.1717). The CellCycleScoring function[47] in Seurat was applied to calculate the scores of cell-cycle phases. For this, the following filter conditions were applied: nFeature_RNA = more than 4,000 and less than 100; nCount = more than 20,000, and percent_mt = more than 15%. nFeature_RNA represents the number of all genes detected in each cell; nCount_RNA represents the sum of the expression level of all genes in each cell; and percent.it represents the proportion of mitochondrial genes detected in each cell. A total of 4,377 cells were used for the downstream analysis. The transform normalization workflow[48] was adopted to mitigate possible technically driven or other variations, in which mitochondrial genes and cell-cycle phase were regressed out. Uniform Manifold Approximation and Projection was used for converting cells into two-dimensional maps. The FindAllMarkers function was performed to detect the main features of each cluster with default parameters. The top expressed genes were used for cell type identification.

Bulk sequencing of AAA patient- and CTRL donor-derived AoSMCs

Commercially available AoSMCs coming from three different non-aneurysmal aorta donors (CTRL, cat. 354-05a, lot 1596 and lot 2991; cat. PB-CH-280-2011, lotQC-19B14F08) *vs.* AoSMCs isolated from five AAA patients (Table S4) were submitted to sequencing analysis (Illumina NovaSeq platform). Three technical replicates were included for each patient/CTRL donor. Cells were collected in QIAzol (QIAGEN) and RNA isolated by taking advantage of the miRNeasy Mini Kit (QIAGEN). RNA was quantified by NanoDrop, and QC was performed using an Agilent 2100 Bioanalyzer (Agilent Technologies). Raw FASTQ files were analyzed using FastQC to assess sequencing quality, GC content, sequence length distribution, and adapter content. Between 48 and 64 million RNA-seq 150 bp pair-end reads were generated for each sample. QC was performed on both raw sequencing files and reads were aligned to human genome GRCh38 using the STAR aligner. A total of 42,513 features with low read counts were filtered using filterbyExpr. Any gene with less than 15 counts in total across all samples or with less than 0.28 CPM in more than 20 samples was filtered out from the edgeR package, resulting in 18,974 features remaining for normalization

and downstream analysis. Raw and normalized expression data were evaluated by several automated outlier detection tests. Exploratory data analysis was performed on the samples pre- and post-normalization. Two samples, AAASMC_86_1 and AoSMC_C_20_1 failed two out of four automated outlier detection tests and were subsequently excluded from the dataset.

Thresholds of fold change in expression >2 and FDR-adjusted $p < 0.001$ produced a set of 661 differentially expressed genes (DEGs). Differential expression and functional enrichment analysis were defined based on expression fold changes between the patient-derived and control cell lines at > 2 and FDR-adjusted $p < 0.001$. Gene set enrichment analysis of Reactome pathways (https://reactome.org) and GO (geneontology.org) terms were eventually performed based on the identified DEGs. In particular, significantly up- and downregulated input genes were mapped to Entrez gene identifiers (n = 633) and assessed via Reactome pathway/GO term over-representation analysis. p values were determined using a hypergeometric test performed using the clusterProfiler package and adjusted for multiple comparisons using the Benjamini-Hochberg method (p(adj.)). Significance was considered as possessing an adjusted $p < 0.05$. An odds ratio was calculated as the number of significant genes observed over that which could be expected by chance. A pathway/term activity *Z* score was calculated as $Z = (Su - Sd)/N - -\sqrt{}$, where N is the total number of genes in the pathway/term, and Su and Sd are the number of significant upregulated and downregulated genes in the pathway/term, respectively. Based on this analysis, statistically significant GO terms and pathways related to apoptosis, proliferation, and cell circle were identified for targeted pathway/GO analysis using R packages "org.Hs.eg.db" and "clusterProfiler." Full outputs of pathway analysis are reported in Tables S2 and S3.

Double immunofluorescence staining

Human AAA/control tissue samples were mounted on poly-L-lysine-pre-coated SuperFrost Plus slides (Thermo Fisher Scientific). Human OCT-embedded frozen tissue was cut into 8 μm thick slides, dried, and stored at −80°C. Fixation was performed in ice-cold acetone for 10 min. For paraffin-embedded samples, fixation was performed for 48 h in 4% paraformaldehyde at room temperature and sections of 3 μm were cut. Only for these samples, deparaffination and antigen retrieval were performed. After blocking of peroxidase activity (0.3% hydrogen peroxide for 15 min), additional blocking with 5% horse serum was performed for 1 h. Primary and secondary antibodies were diluted in 5% horse serum as follows: anti-ATM ab32420 1:100, anti-SMA ab78171:200. Both primary antibodies were incubated after one another overnight at 4°C, followed by secondary antibodies for 1 h each at the respective day. For negative controls, only the secondary antibody was applied for 1 h at room temperature. TrueBlack Lipofuscin Autofluorescence Quencher (Biotium, Fremont, CA) was applied to reduce background fluorescence. Sections were counterstained with DAPI (Thermo Fisher Scientific), and images were taken under a confocal microscope (Olympus FV3000).

IHC

Two micrometer sections of paraffin-embedded tissue were mounted on SuperFrost slides (Thermo Fisher Scientific) and standard hematoxylin and eosin and Elastica van Gieson (EVG) stainings were performed. For IHC, sections were mounted on 0.1% poly-L-lysine (Sigma-Aldrich, St. Louis, MO) pre-coated SuperFrost Plus slides (Thermo Fisher Scientific). For antigen retrieval, slides were boiled in a pressure cooker with 10 nM citrate buffer (distilled water with citric acid monohydrate [pH 6.0]), and endogenous peroxidase activity was blocked with 3% hydrogen peroxide. Consecutive slides were incubated with anti-ATM (1:100) or anti-SMA (1:200) diluted in Dako REAL Antibody Diluent (Dako, Glostrup, Denmark). Slides were then treated with biotinylated secondary antibodies and target staining was performed with peroxidase-conjugated streptavidin and DAB chromogen (Dako REAL Detection System Peroxidase/DAB+, Rabbit/Mouse Kit; Dako). Mayer's hematoxylin (Carl Roth, Karlsruhe, Germany) was used for counterstaining and appropriate positive and negative controls were performed for each antibody. All slides were scanned with an Aperio AT2 (Leica, Wetzlar, Germany), and images were taken with the Aperio ImageScope software (Leica).

ISH

QIAGEN miRCURY locked nucleic acid DIG (digoxigenin)-labeled probes (sense *cATM*-DIG: 5′ DIG-AGTGGTTAGACAGTGATG TGT-DIG 3′) (QIAGEN) were used for ISH, performed according to the manufacturer's instructions. A complete list of ISH probes sequences is reported in Table S7. In brief, tissue sections were either de-paraffinized (formalin-fixed paraffin-embedded) or thawed (frozen) and rehydrated. After proteinase K permeabilization, *cATM* probe hybridization was carried out at 54°C for 2 h in a hybridization oven. A negative control (no probe) was performed in parallel. Slides were washed in pre-wormed saline sodium citrate buffers at hybridization temperature, with subsequent DIG detection methods as described previously.[49] Nuclear counterstaining was performed with Nuclear Fast Red (Sigma-Aldrich).

Protein isolation and western blotting

Cells were homogenized in RIPA buffer (Thermo Fisher Scientific) including protease and phosphatase inhibitor cocktails (Sigma-Aldrich). Protein concentrations were determined using the Bicinchoninic Acid assay (Thermo Fisher Scientific), following the manufacturer's protocol. Protein samples (10–40 μg/well) were mixed with LDS 4× Sample Buffer (Novex) and sample reducing agent (Novex), denatured at 95°C for 5 min and loaded on NuPage 3%–8% or 4%–12% gels. Following electrophoresis and electrotransfer, blots were blocked with 5% milk in Tris-buffered saline + 0.1% Tween 20 and probed with specific antibodies diluted in blocking solution. Signals were revealed after incubation with horseradish peroxidase (HRP)-conjugated secondary antibodies (Abcam) 1:10,000, in combination with ECL (GE Healthcare). Image detection was performed with C600 Azure Biosystems Imager (Biozym)/ChemiDoc XRS System (Bio-Rad, Hercules, CA) and image quantification was carried out with ImageJ software.

Employed antibodies were all diluted in 5% milk in TBS-T as follows: β-actin no. A1978 (Sigma), 1:10,000; ATM no. ab32420 1:500; p53 no. ab131442 1:1,000; phospho-p53 no. ab1431 1:500; phospho-ATM no. ab81292 1:500; MY11C no. ab53219 1:500; β-tubulin no. ab6046; caspase-3 no. ab13837 1:250; active caspase-3 no. 5A1E (Cell Signaling; BCL-2 no. ab32124 1:1,000).

Cell fractionation

Nucleocytoplasmic fractionation was performed as described previously.[50] Fractions were extracted from confluent hAoSMCs cultured in T75cm2-flasks (Corning) and RNA isolated using QIAzol reagent, as explained above. The purity of the nuclear and cytoplasmic fractions was confirmed by real-time quantitative PCR on *GAPDH/RPLPO/ß Actin* and *NEAT1*, respectively.

Kinetic assessment of proliferation and apoptosis in human AoSMCs

Real-time assessment of hAoSMCs status was carried out with an IncuCyte Zoom System (Sartorius, Goettingen, Germany), as described previously by our group.[51,52] Live-cell imaging was performed upon target silencing or doxorubicin treatment. To evaluate the death rate, a caspase-3/7 apoptosis reagent (Sartorius) was added at a final concentration of 5 μM prior to imaging with phase contrast/fluorescence (4 h/imaging pattern). Images were auto-collected and analyzed by using the IncuCyte software package.

ATM enzyme-linked immunoassay

ATM enzyme-linked immunoassay was performed on 7 PAD *vs.* 7 AAA patient serum samples according to the manufacturer's instructions (NBP2_69891, Novus Biologicas). In brief, 80 μL of standard or serum were aliquoted into anti-ATM-coated wells in duplicate and incubated. After application of biotinylated antibody, wells were washed and provided with HRP conjugate. After further washings, the signal was revealed via substrate addition and stopped after 15 min. Absorbance was read at 450 nm with a plate reader (Molecular Devices, Germany).

Statistical analysis

All data are expressed as means ± SD or ± SEM for $n \geq 3$ replicas. Statistical analysis was performed by using GraphPad Prism software. Statistically significant differences were assessed by Student's t test. Values of $p < 0.05$ were considered significant.

DATA AND CODE AVAILABILITY

Array, single-cell, and bulk RNA sequencing data have been deposited in the GEO under accession nos. GSE236869, GSE237230, and GSE237229.

SUPPLEMENTAL INFORMATION

Supplemental information can be found online at https://doi.org/10.1016/j.omtn.2023.08.017.

ACKNOWLEDGMENTS

We are indebted to all the members of the Molecular Vascular Medicine lab at the Technical University Munich for thought-provoking discussions. We thank Renate Hegenloh and the Munich Vascular Biobank team for technical support with human specimens. We are grateful to Dongchao Lu for his advice regarding c*ATM* vector construction. We thank Joscha Büch for kindly providing RNA from TAA tissue during the revision process. This work was supported by funding from the Swedish Heart-Lung Foundation (20210450), the Swedish Research Council (Vetenkapsrådet, 2019-01577), a DZHK Translational Research Project on microRNA modulation in aortic aneurysms, the CRC1123 and TRR267 of the German Research Council (DFG), the National Institutes of Health (NIH; 1R011HL150359-01), and the Bavarian State Ministry of Health and Care through the research project DigiMed Bayern.

AUTHOR CONTRIBUTIONS

L.M. and F.F. conceived and designed the project and wrote the manuscript. F.F. supervised the research, executed the experiments, and analyzed and interpreted the data. G.W. designed and executed the experiments, curated and analyzed the data, and participated in data interpretation. Z.W., Z.L., J.R., H.W., J.P., R.A.B., V.P., and N.G. assisted with the experiments and data collection and analyzed the data. H.H.E., A.B., C.K., and N.S. collected and provided human specimens (Munich Vascular Biobank). R.H. and J.R. collected and provided human specimens (Stockholm Aortic Aneurysm Biobank).

DECLARATION OF INTERESTS

L.M. is a scientific consultant and adviser for Novo Nordisk (Malov, Denmark), DrugFarm (Shanghai, China), and Angiolutions (Hannover, Germany), and received research funds from Roche Diagnostics (Rotkreuz, Switzerland).

REFERENCES

1. Sakalihasan, N., Michel, J.-B., Katsargyris, A., Kuivaniemi, H., Defraigne, J.-O., Nchimi, A., Powell, J.T., Yoshimura, K., and Hultgren, R. (2018). Abdominal aortic aneurysms. Nat. Rev. Dis. Prim. *4*, 34. https://doi.org/10.1038/s41572-018-0030-7.
2. Yuan, Z., Lu, Y., Wei, J., Wu, J., Yang, J., and Cai, Z. (2020). Abdominal Aortic Aneurysm: Roles of Inflammatory Cells. Front. Immunol. *11*, 609161. https://doi.org/10.3389/fimmu.2020.609161.
3. McCormick, M.L., Gavrila, D., and Weintraub, N.L. (2007). Role of oxidative stress in the pathogenesis of abdominal aortic aneurysms. Arterioscler. Thromb. Vasc. Biol. *27*, 461–469. https://doi.org/10.1161/01.ATV.0000257552.94483.14.
4. Golledge, J., and Norman, P.E. (2011). Current status of medical management for abdominal aortic aneurysm. Atherosclerosis *217*, 57–63. https://doi.org/10.1016/j.atherosclerosis.2011.03.006.
5. Schanzer, A., and Oderich, G.S. (2021). Management of Abdominal Aortic Aneurysms. N. Engl. J. Med. *385*, 1690–1698. https://doi.org/10.1056/NEJMcp2108504.
6. Kristensen, L.S., Andersen, M.S., Stagsted, L.V.W., Ebbesen, K.K., Hansen, T.B., and Kjems, J. (2019). The biogenesis, biology and characterization of circular RNAs. Nat. Rev. Genet. *20*, 675–691. https://doi.org/10.1038/s41576-019-0158-7.
7. Zhang, X.O., Wang, H.B., Zhang, Y., Lu, X., Chen, L.L., and Yang, L. (2014). Complementary sequence-mediated exon circularization. Cell *159*, 134–147. https://doi.org/10.1016/j.cell.2014.09.001.
8. Suzuki, H., Zuo, Y., Wang, J., Zhang, M.Q., Malhotra, A., and Mayeda, A. (2006). Characterization of RNase R-digested cellular RNA source that consists of lariat

and circular RNAs from pre-mRNA splicing. Nucleic Acids Res. *34*, e63. https://doi.org/10.1093/nar/gkl151.

9. Kjems, J., and Garrett, R.A. (1988). Novel splicing mechanism for the ribosomal RNA intron in the archaebacterium Desulfurococcus mobilis. Cell *54*, 693–703. https://doi.org/10.1016/s0092-8674(88)80014-x.

10. Yu, C.-Y., and Kuo, H.-C. (2019). The emerging roles and functions of circular RNAs and their generation. J. Biomed. Sci. *26*, 29. https://doi.org/10.1186/s12929-019-0523-z.

11. Zhang, Z., Yang, T., and Xiao, J. (2018). Circular RNAs: Promising Biomarkers for Human Diseases. EBioMedicine *34*, 267–274. https://doi.org/10.1016/j.ebiom.2018.07.036.

12. Holdt, L.M., Stahringer, A., Sass, K., Pichler, G., Kulak, N.A., Wilfert, W., Kohlmaier, A., Herbst, A., Northoff, B.H., Nicolaou, A., et al. (2016). Circular non-coding RNA ANRIL modulates ribosomal RNA maturation and atherosclerosis in humans. Nat. Commun. *7*, 12429. https://doi.org/10.1038/ncomms12429.

13. Burd, C.E., Jeck, W.R., Liu, Y., Sanoff, H.K., Wang, Z., and Sharpless, N.E. (2010). Expression of linear and novel circular forms of an INK4/ARF-associated non-coding RNA correlates with atherosclerosis risk. PLoS Genet. *6*, e1001233. https://doi.org/10.1371/journal.pgen.1001233.

14. Fasolo, F., Di Gregoli, K., Maegdefessel, L., and Johnson, J.L. (2019). Non-coding RNAs in cardiovascular cell biology and atherosclerosis. Cardiovasc. Res. *115*, 1732–1756. https://doi.org/10.1093/cvr/cvz203.

15. Zhang, C., Huo, S.T., Wu, Z., Chen, L., Wen, C., Chen, H., Du, W.W., Wu, N., Guan, D., Lian, S., and Yang, B.B. (2020). Rapid Development of Targeting circRNAs in Cardiovascular Diseases. Mol. Ther. Nucleic Acids *21*, 568–576. https://doi.org/10.1016/j.omtn.2020.06.022.

16. He, X., Li, X., Han, Y., Chen, G., Xu, T., Cai, D., Sun, Y., Wang, S., Lai, Y., Teng, Z., et al. (2022). CircRNA Chordc1 protects mice from abdominal aortic aneurysm by contributing to the phenotype and growth of vascular smooth muscle cells. Mol. Ther. Nucleic Acids *27*, 81–98. https://doi.org/10.1016/j.omtn.2021.11.005.

17. Heumüller, A.W., Jones, A.N., Mourão, A., Klangwart, M., Shi, C., Wittig, I., Fischer, A., Muhly-Reinholz, M., Buchmann, G.K., Dieterich, C., et al. (2022). Locus-Conserved Circular RNA cZNF292 Controls Endothelial Cell Flow Responses. Circ. Res. *130*, 67–79. https://doi.org/10.1161/CIRCRESAHA.121.320029.

18. Wang, X., Li, H., Lu, Y., and Cheng, L. (2020). Regulatory Effects of Circular RNAs on Host Genes in Human Cancer. Front. Oncol. *10*, 586163. https://doi.org/10.3389/fonc.2020.586163.

19. Lu, H., Du, W., Ren, L., Hamblin, M.H., Becker, R.C., Chen, Y.E., and Fan, Y. (2021). Vascular Smooth Muscle Cells in Aortic Aneurysm: From Genetics to Mechanisms. J. Am. Heart Assoc. *10*, e023601. https://doi.org/10.1161/JAHA.121.023601.

20. Forsdahl, S.H., Singh, K., Solberg, S., and Jacobsen, B.K. (2009). Risk factors for abdominal aortic aneurysms: a 7-year prospective study: the Tromsø Study, 1994-2001. Circulation *119*, 2202–2208. https://doi.org/10.1161/circulationaha.108.817619.

21. Vardulaki, K.A., Prevost, T.C., Walker, N.M., Day, N.E., Wilmink, A.B., Quick, C.R., Ashton, H.A., and Scott, R.A. (1999). Incidence among men of asymptomatic abdominal aortic aneurysms: estimates from 500 screen detected cases. J. Med. Screen *6*, 50–54. https://doi.org/10.1136/jms.6.1.50.

22. Lederle, F.A., Johnson, G.R., Wilson, S.E., Littooy, F.N., Krupski, W.C., Bandyk, D., Acher, C.W., Chute, E.P., Hye, R.J., Gordon, I.L., et al. (2000). Yield of repeated screening for abdominal aortic aneurysm after a 4-year interval. Aneurysm Detection and Management Veterans Affairs Cooperative Study Investigators. Arch. Intern. Med. *160*, 1117–1121. https://doi.org/10.1001/archinte.160.8.1117.

23. Wilmink, A.B., Hubbard, C.S., Day, N.E., and Quick, C.R. (2001). The incidence of small abdominal aortic aneurysms and the change in normal infrarenal aortic diameter: implications for screening. Eur. J. Vasc. Endovasc. Surg. *21*, 165–170. https://doi.org/10.1053/ejvs.2000.1285.

24. Sanger, H.L., Klotz, G., Riesner, D., Gross, H.J., and Kleinschmidt, A.K. (1976). Viroids are single-stranded covalently closed circular RNA molecules existing as highly base-paired rod-like structures. Proc. Natl. Acad. Sci. USA *73*, 3852–3856. https://doi.org/10.1073/pnas.73.11.3852.

25. Patop, I.L., Wüst, S., and Kadener, S. (2019). Past, present, and future of circRNAs. EMBO J. *38*, e100836. https://doi.org/10.15252/embj.2018100836.

26. Lee, E.C.S., Elhassan, S.A.M., Lim, G.P.L., Kok, W.H., Tan, S.W., Leong, E.N., Tan, S.H., Chan, E.W.L., Bhattamisra, S.K., Rajendran, R., and Candasamy, M. (2019). The roles of circular RNAs in human development and diseases. Biomed. Pharmacother. *111*, 198–208. https://doi.org/10.1016/j.biopha.2018.12.052.

27. Verduci, L., Tarcitano, E., Strano, S., Yarden, Y., and Blandino, G. (2021). CircRNAs: role in human diseases and potential use as biomarkers. Cell Death Dis. *12*, 468. https://doi.org/10.1038/s41419-021-03743-3.

28. Hellenthal, F.A.M.V.I., Buurman, W.A., Wodzig, W.K.W.H., and Schurink, G.W.H. (2009). Biomarkers of AAA progression. Part 1: extracellular matrix degeneration. Nat. Rev. Cardiol. *6*, 464–474. https://doi.org/10.1038/nrcardio.2009.80.

29. Szabo, L., and Salzman, J. (2016). Detecting circular RNAs: bioinformatic and experimental challenges. Nat. Rev. Genet. *17*, 679–692. https://doi.org/10.1038/nrg.2016.114.

30. Yu, Z., Huang, Q., Zhang, Q., Wu, H., and Zhong, Z. (2021). CircRNAs open a new era in the study of cardiovascular disease (Review). Int. J. Mol. Med. *47*, 49–64. https://doi.org/10.3892/ijmm.2020.4792.

31. Blunder, S., Messner, B., Scharinger, B., Doppler, C., Zeller, I., Zierer, A., Laufer, G., and Bernhard, D. (2018). Targeted gene expression analyses and immunohistology suggest a pro-proliferative state in tricuspid aortic valve-and senescence and viral infections in bicuspid aortic valve-associated thoracic aortic aneurysms. Atherosclerosis *271*, 111–119. https://doi.org/10.1016/j.atherosclerosis.2018.02.007.

32. Oshima, T., Hara, H., Takeda, N., Hasumi, E., Kuroda, Y., Taniguchi, G., Inuzuka, R., Nawata, K., Morita, H., and Komuro, I. (2017). A novel mutation of NFIX causes Sotos-like syndrome (Malan syndrome) complicated with thoracic aortic aneurysm and dissection. Hum. Genome Var. *4*, 17022. https://doi.org/10.1038/hgv.2017.22.

33. Parmacek, M.S. (2008). Myocardin: dominant driver of the smooth muscle cell contractile phenotype. Arterioscler. Thromb. Vasc. Biol. *28*, 1416–1417. https://doi.org/10.1161/ATVBAHA.108.168930.

34. Rol, N., Kurakula, K.B., Happé, C., Bogaard, H.J., and Goumans, M.J. (2018). TGF-β and BMPR2 Signaling in PAH: Two Black Sheep in One Family. Int. J. Mol. Sci. *19*, 2585. https://doi.org/10.3390/ijms19092585.

35. Liu, X., Guo, J.-W., Lin, X.-C., Tuo, Y.-H., Peng, W.-L., He, S.-Y., Li, Z.-Q., Ye, Y.-C., Yu, J., Zhang, F.-R., et al. (2021). Macrophage NFATc3 prevents foam cell formation and atherosclerosis: evidence and mechanisms. Eur. Heart J. *42*, 4847–4861. https://doi.org/10.1093/eurheartj/ehab660.

36. Li, X., Yang, L., and Chen, L.-L. (2018). The Biogenesis, Functions, and Challenges of Circular RNAs. Mol. Cell *71*, 428–442. https://doi.org/10.1016/j.molcel.2018.06.034.

37. Lovejoy, C.A., and Cortez, D. (2009). Common mechanisms of PIKK regulation. DNA Repair *8*, 1004–1008. https://doi.org/10.1016/j.dnarep.2009.04.006.

38. Li, C., Zhu, L., Fu, L., Han, M., Li, Y., Meng, Z., and Qiu, X. (2021). CircRNA NRIP1 promotes papillary thyroid carcinoma progression by sponging mir-195-5p and modulating the P38 MAPK and JAK/STAT pathways. Diagn. Pathol. *16*, 93. https://doi.org/10.1186/s13000-021-01153-9.

39. Carlessi, L., De Filippis, L., Lecis, D., Vescovi, A., and Delia, D. (2009). DNA-damage response, survival and differentiation *in vitro* of a human neural stem cell line in relation to ATM expression. Cell Death Differ. *16*, 795–806. https://doi.org/10.1038/cdd.2009.10.

40. Der, S.D., Yang, Y.L., Weissmann, C., and Williams, B.R. (1997). A double-stranded RNA-activated protein kinase-dependent pathway mediating stress-induced apoptosis. Proc. Natl. Acad. Sci. USA *94*, 3279–3283. https://doi.org/10.1073/pnas.94.7.3279.

41. Estornes, Y., Toscano, F., Virard, F., Jacquemin, G., Pierrot, A., Vanbervliet, B., Bonnin, M., Lalaoui, N., Mercier-Gouy, P., Pachéco, Y., et al. (2012). dsRNA induces apoptosis through an atypical death complex associating TLR3 to caspase-8. Cell Death Differ. *19*, 1482–1494. https://doi.org/10.1038/cdd.2012.22.

42. Qian, G., Adeyanju, O., Olajuyin, A., and Guo, X. (2022). Abdominal Aortic Aneurysm Formation with a Focus on Vascular Smooth Muscle Cells. Life *12*, 191.

43. Schmittgen, T.D., and Livak, K.J. (2008). Analyzing real-time PCR data by the comparative C(T) method. Nat. Protoc. *3*, 1101–1108. https://doi.org/10.1038/nprot.2008.73.

44. Coulter, S.J. (2018). Mitigation of the effect of variability in digital PCR assays through use of duplexed reference assays for normalization. Biotechniques *65*, 86–91. https://doi.org/10.2144/btn-2018-0058.

45. Butler, A., Hoffman, P., Smibert, P., Papalexi, E., and Satija, R. (2018). Integrating single-cell transcriptomic data across different conditions, technologies, and species. Nat. Biotechnol. *36*, 411–420. https://doi.org/10.1038/nbt.4096.

46. Stuart, T., Butler, A., Hoffman, P., Hafemeister, C., Papalexi, E., Mauck, W.M., 3rd, Hao, Y., Stoeckius, M., Smibert, P., and Satija, R. (2019). Comprehensive Integration of Single-Cell Data. Cell *177*, 1888–1902.e21. https://doi.org/10.1016/j.cell.2019.05.031.

47. Barron, M., and Li, J. (2016). Identifying and removing the cell-cycle effect from single-cell RNA-Sequencing data. Sci. Rep. *6*, 33892. https://doi.org/10.1038/srep33892.

48. Hafemeister, C., and Satija, R. (2019). Normalization and variance stabilization of single-cell RNA-seq data using regularized negative binomial regression. Genome Biol. *20*, 296. https://doi.org/10.1186/s13059-019-1874-1.

49. Fasolo, F., Jin, H., Winski, G., Chernogubova, E., Pauli, J., Winter, H., Li, D.Y., Glukha, N., Bauer, S., Metschl, S., et al. (2021). Long Noncoding RNA MIAT Controls Advanced Atherosclerotic Lesion Formation and Plaque Destabilization. Circulation *144*, 1567–1583. https://doi.org/10.1161/CIRCULATIONAHA.120.052023.

50. Wang, Y., Zhu, W., and Levy, D.E. (2006). Nuclear and cytoplasmic mRNA quantification by SYBR green based real-time RT-PCR. Methods *39*, 356–362. https://doi.org/10.1016/j.ymeth.2006.06.010.

51. Jin, H., Li, D.Y., Chernogubova, E., Sun, C., Busch, A., Eken, S.M., Saliba-Gustafsson, P., Winter, H., Winski, G., Raaz, U., et al. (2018). Local Delivery of miR-21 Stabilizes Fibrous Caps in Vulnerable Atherosclerotic Lesions. Mol. Ther. *26*, 1040–1055. https://doi.org/10.1016/j.ymthe.2018.01.011.

52. Li, D.Y., Busch, A., Jin, H., Chernogubova, E., Pelisek, J., Karlsson, J., Sennblad, B., Liu, S., Lao, S., Hofmann, P., et al. (2018). H19 Induces Abdominal Aortic Aneurysm Development and Progression. Circulation *138*, 1551–1568. https://doi.org/10.1161/CIRCULATIONAHA.117.032184.

OMTN, Volume *33*

Supplemental information

The circular RNA Ataxia Telangiectasia Mutated regulates oxidative stress in smooth muscle cells in expanding abdominal aortic aneurysms

Francesca Fasolo, Greg Winski, Zhaolong Li, Zhiyan Wu, Hanna Winter, Julia Ritzer, Nadiya Glukha, Joy Roy, Rebecka Hultgren, Jessica Pauli, Albert Busch, Nadja Sachs, Christoph Knappich, Hans-Henning Eckstein, Reinier A. Boon, Valentina Paloschi, and Lars Maegdefessel

Table S1. Summary of all statistically significant up-and downregulated circRNAs as of array analysis *(excel spreadsheet).*

Table S2. **Full output of Reactome pathway analysis** *(excel spreadsheet).*

Table S3. Full output of Gene ontology analysis *(excel spreadsheet).*

Table S4. List and features of all patient samples used in this study *(excel spreadsheet).*

Table S5. **List of PCR oligonucleotides and Taqman assays used in this study**.

Primer ID	**Sequence (5´-->3´)**	**Company**
ATM_1_F	CGTGGCTAACGGAGAAAAGA	ThermoFisher
ATM_1_R	ACTGCACTCGGAAGGTCAAA	ThermoFisher
circNRIP1_F	TCCGGATGACATCAGAGCTA	ThermoFisher
circNRIP1_R	TGTGCATCTTCTGGCTGTGT	ThermoFisher
circSLIT33_F (hsa_circ_0074930)	GCACGTGCAGCAATAACATC	ThermoFisher
circSLIT33_R (hsa_circ_0074930)	ATCTTCGGCATGTGGTTGA	ThermoFisher
hsa_circ_0003218 _F (cBMPR2)	CCGTTTCTGCTGTTGTAGCA	ThermoFisher
hsa_circ_0003218 _R (cBMPR2)	CCTATCCCAAGGTCTTGCTG	ThermoFisher
hsa_circ_0003641_F (cATM)	TGGTGCTATTTACGGAGCTG	ThermoFisher
hsa_circ_0003641_R (cATM)	ACGGCAGCAGATAAGCAGAT	ThermoFisher
hsa_circ_0005615_F (cNFATC3)	CACCCTTTACCTGGAGCAAA	ThermoFisher
hsa_circ_0005615_R (cNFATC3)	TGGTAAGCAAAGTGGTGTGG	ThermoFisher
hsa_circ_0005660_F (cNFIX)	CAGCCACATCACATTGGAGT	ThermoFisher
hsa_circ_0005660_R (cNFIX)	TGCAGGTTGAACCAGGTGTA	ThermoFisher
hsa_circ_0008068_F	TGATGAAGCTTTGCGAAGAA	ThermoFisher
hsa_circ_0008068_R	TATGCCCTTCTTGGAAATTACG	ThermoFisher
hsa_circ_0016661 _R (cENAH)	GAATCCAGTTGAGCCACCAG	ThermoFisher
hsa_circ_0016661_F (cENAH)	CCATCCCAAGAAGAATTGGA	ThermoFisher
hsa_circ_0024824_F (cSTGAL4)	TCTCAACCCCTTCTTCATGG	ThermoFisher
hsa_circ_0024824_R (cSTGAL4)	GCTGACCATGTTTCTCAGCA	ThermoFisher
hsa_circ_0042103_F (cMYOCD)	TTCCTGTGGATTCTGCTGTG	ThermoFisher
hsa_circ_0042103_R (cMYOCD)	GGAATTCAGCTGGACGTTTC	ThermoFisher
hsa_circ_0073492 _F (cPAM)	CTCGAGCCAGCATGGATAC	ThermoFisher
hsa_circ_0073492 _R (cPAM)	TTATGACTCCGGAATGACAGG	ThermoFisher
hsa_circ_0075671_F (cJARID)	CATCCCAAGTGTCCTCCACT	ThermoFisher

hsa_circ_0075671_R (cJARID)	ATGCTGCCTCTTCTGGGAAT	ThermoFisher
RPLPO_human_Fwd	ATGGCAGCATCTACAACCCT	ThermoFisher
RPLPO_human_Rev	TTGGGTAGCCAATCTGCAGA	ThermoFisher
Taqman Assay	**Assay ID**	**Company**
MYOCD	Hs00538076_m1	ThermoFisher
NEAT1	HS03453535_S1	ThermoFisher
NFATC3	Hs01001566_m1	ThermoFisher
NFIX	Hs00958846_m1	ThermoFisher
NRIP1	Hs00940781	ThermoFisher
RPLPO	HS99999902	ThermoFisher
RPLPO	HS00420895_gH	ThermoFisher
Custom Taqman Assay	**Assay details**	**Sequence**
circATM	Fwd	TGGTGCTATTTACGGAGCTG
	Rev	ACGGCAGCAGATAAGCAGAT
	Probe	TGTGTTCTGAAATTGTGAACCA
circBMPR2	Fwd	TGGAACATACCGTTTCTGCT
	Rev	CCTATCCCAAGGTCTTGCTG
	Probe	CCACTCACTTCGCAGAATCA
circNFIX	Fwd	CAGCCACATCACATTGGAGT
	Rev	TCTTGAAGTACTTGCGCTTCC
	Probe	TACACCTGGTTCAACCTGC
circNRIP1	Fwd	CTCCGGATGACATCAGAGCT
	Rev	TCTGGCTGTGTTTCTCCCAA
	Probe	GCTCAGAGCTTGGAGACAGA
circNFATC3	Fwd	GTTTCTTTCAGTTCCTTCACCCT
	Rev	TGGTAAGCAAAGTGGTGTGG
	Probe	CCTGGCCACACCCCTATATT
circMYOCD	Fwd	TTCCTGTGGATTCTGCTGTG
	Rev	GGAATTCAGCTGGACGTTTC
	Probe	GGACCCAGGAACAACTGGCTAACCA

Table S6. Template file for digital PCR data analysis *(excel spreadsheet).*

Table S7. **List of oligonucleotides for silencing and *in situ* hybridization.**

siRNA ID	**Cat. Number**	**Company**
Human *ATM* esisrna1	EHU089521	Sigma Aldrich
Custom made siRNA	**Sequence**	**Company**
sicATM_2	AGTGGTTAGACAGTGATGTGT	Sigma Aldrich
sicATM_1	GGTTAGACAGTGATGTGTGTT	Sigma Aldrich
ISH probes	**Details**	**Company**
Sense_c*ATM*	DIG: 5´DIG-AGTGGTTAGACAGTGATGTGT-DIG 3´	Exiqon

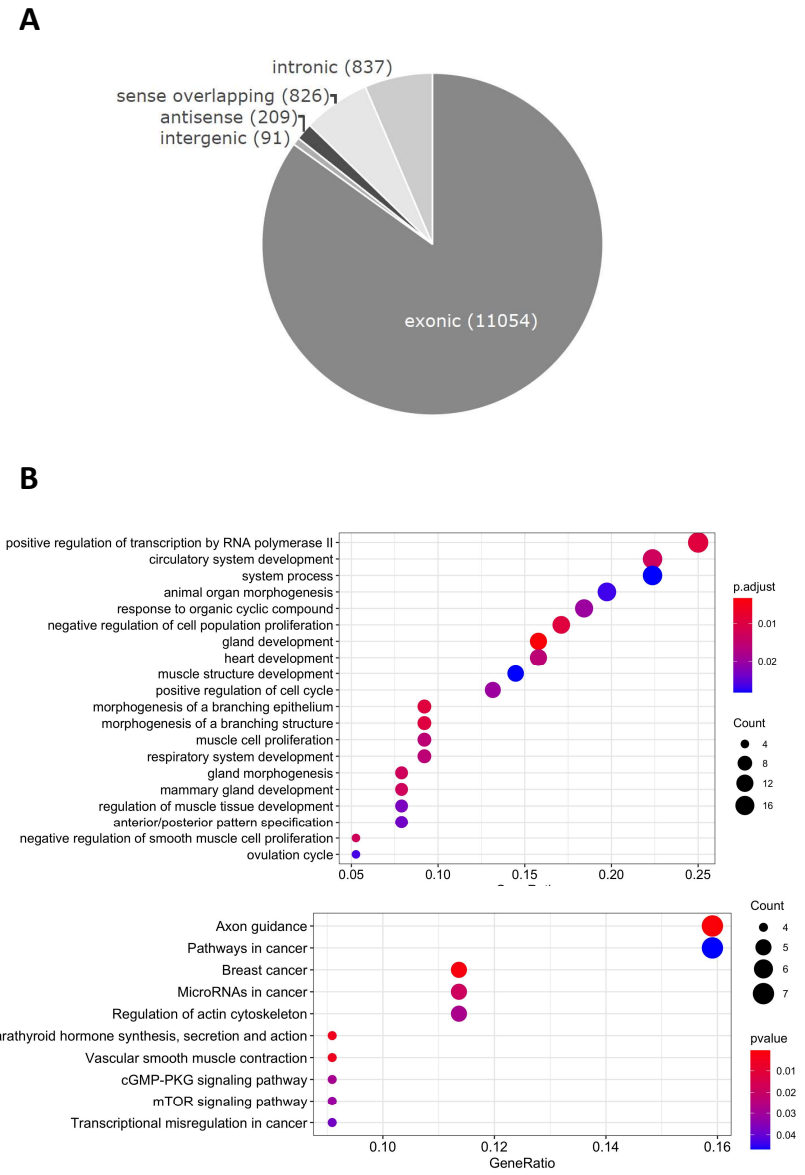

Figure S1. ***Differentially expressed circRNAs in eAAA vs CTRL patients*****. A.** Pie chart illustrating the proportion of exonic, intronic, sense-overlapping and antisense circRNAs in all (13.617) circRNAs covered by one array chip. Absolute numbers are further indicated for each group. **B.** Top: Gene Ontology (GO) and pathway enrichment analysis relative to linear mRNA counterparts of differentially expressed exonic circRNAs. Top significantly enriched (adjusted p value < 0.05) GO-terms/ pathways are shown. Abbr: eAAA: elective AAA; CTRL: control.

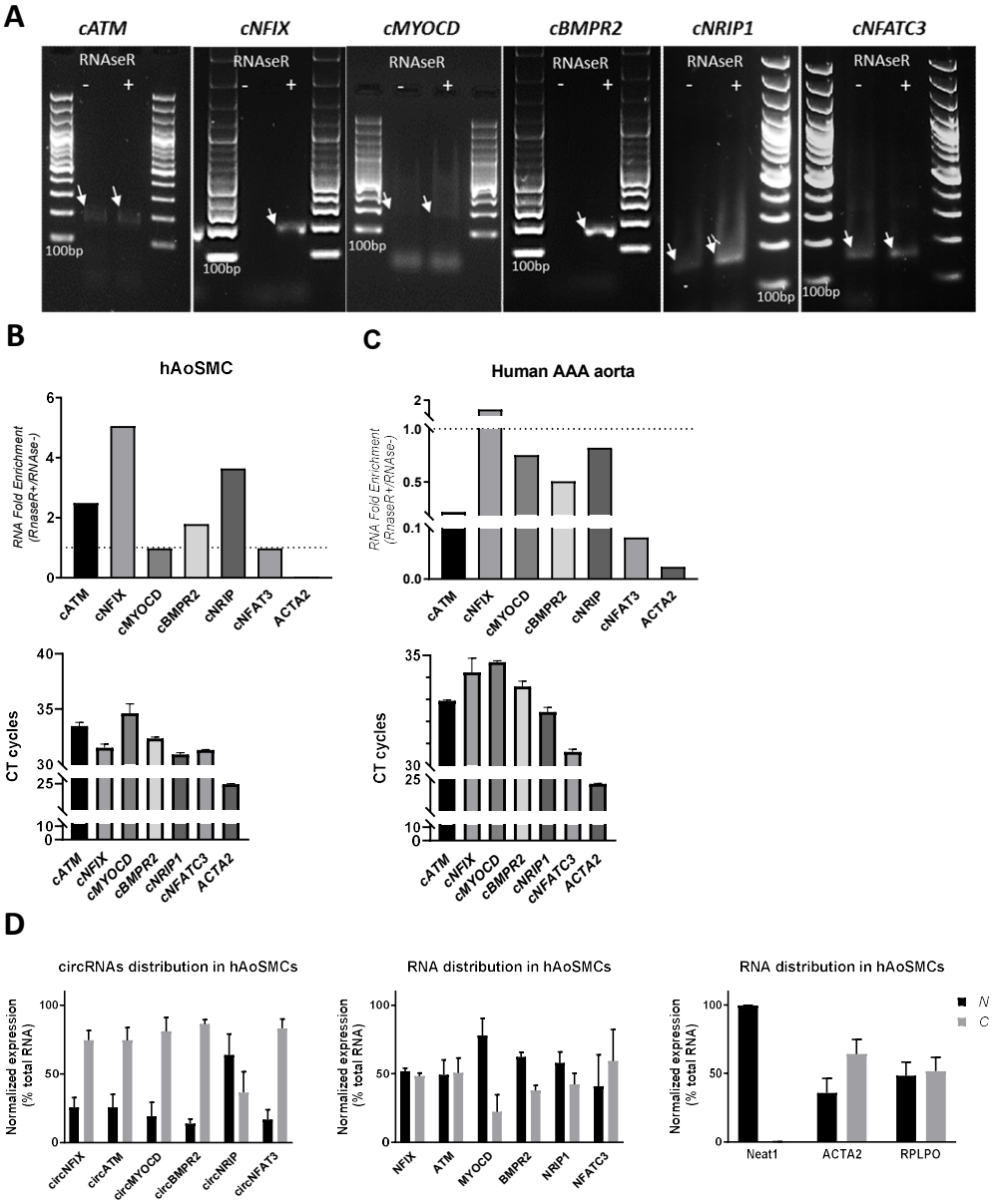

Figure S2. ***Validation of circular junctions in human aortic smooth muscle cells and human abdominal aortic aneurysm tissue specimens.*** **A.** circRNAs amplicons obtained from PCR on hAoSMCs cDNA were cloned and submitted to Sanger sequencing. Enrichment upon RNAseR treatment is shown (lane labelled with +). **B** and **C**, top: RNA fold enrichment upon RNAseR treatment in hAoSMCs and AAA tissue. Fold enrichment was calculated by comparing CT values in RNAseR+ *vs* RNAseR- and expressed as 2^-delta CT*100, with delta CT= CT RNAseR+ - CT RNAseR-. Targets displaying values >1 are considered enriched. Bottom: average CT cycles of the six circRNA targets compared to housekeeping gene (*ACTA2*) in untreated conditions. **D.** Subcellular localization of circRNAs (left) and respective linear counterpart (middle) in AoSMCs as quantified by qRT-PCR. Nuclear (abbr.: N) and cytoplasm (abbr.: C) purity was monitored by measuring *ACTA2/ RPLPO* or *NEAT1*, respectively (right). Expression levels are indicated as percentage of total RNA. Data are represented as mean ± SEM; N=3. Abbr.: hAoSMCs= human aortic smooth muscle cells; AAA= abdominal aortic aneurysm.

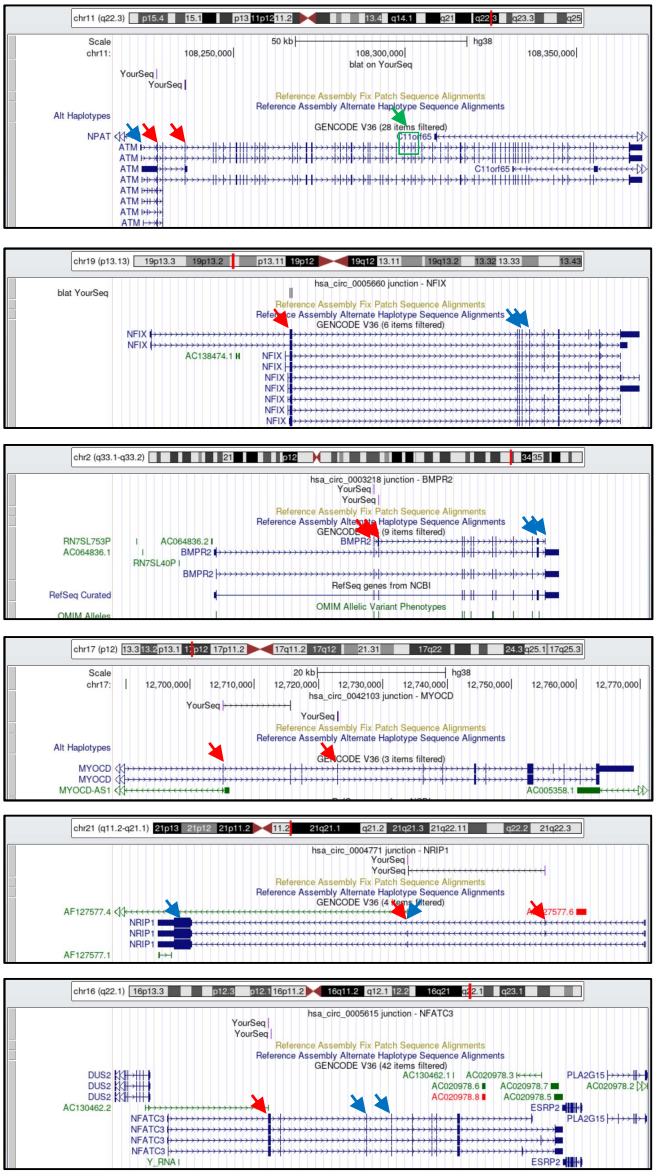

Figure S3. ***Genome Browser view of host gene loci of validated circRNA targets*.** Red arrows indicate exons involved in backsplicing. Taqman assays and siRNAs targeting circRNAs were designed on the backsplicing junction. Taqman assays/ primers for detection of linear transcripts map on blue arrows. SiRNAs target sites of linear transcripts are indicated by green arrows.

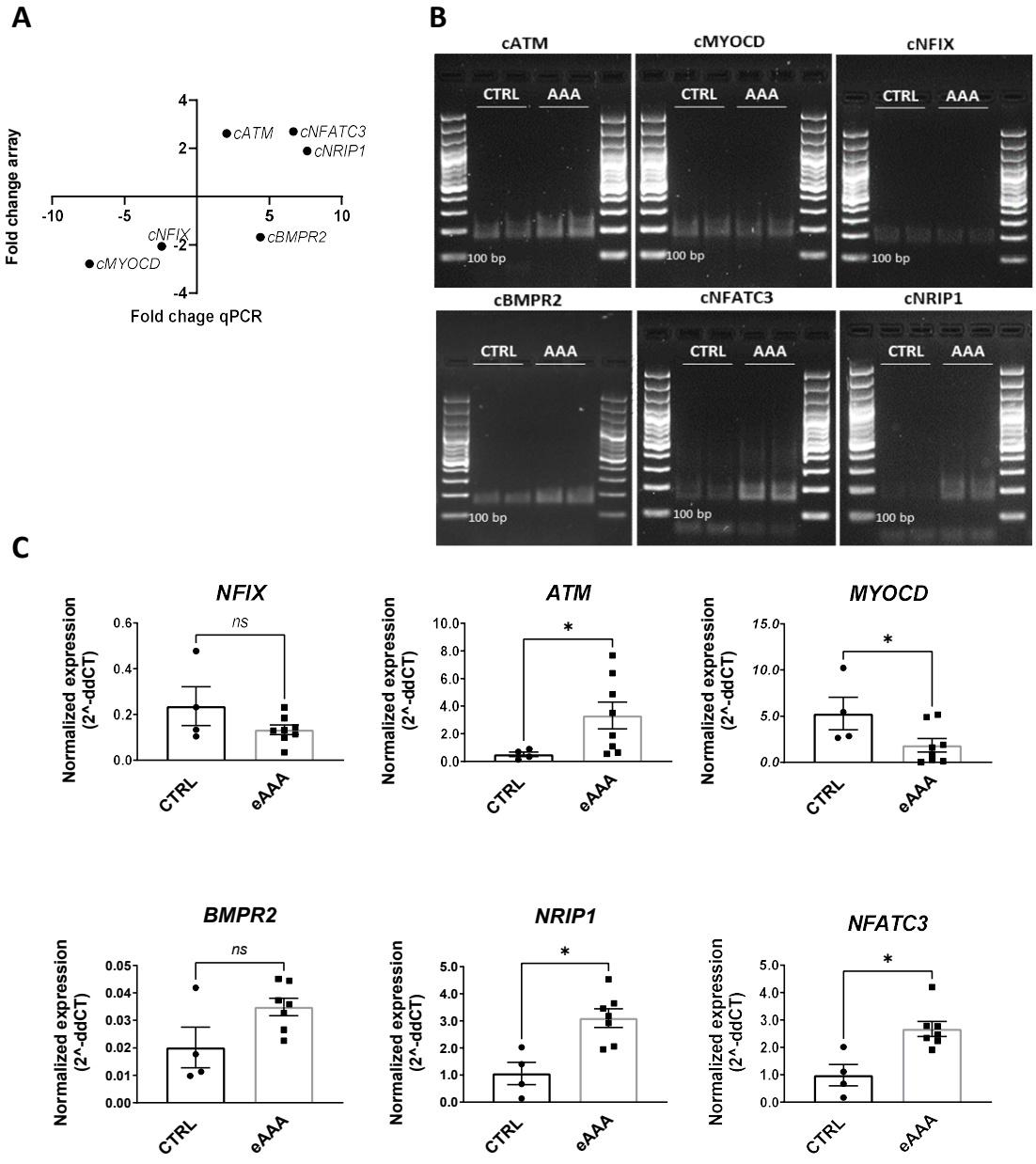

Figure S4. ***Expression of circRNAs chosen for validation and of their linear counterparts in eAAA vs CTRL patients***. **A.** Correlation plot comparing array *vs.* qPCR results relative to the six circRNA targets chosen for validation. Array *vs* qPCR fold changes are plotted. Statistics: Pearson r; R squared: 0.5546; p value (two-tailed): 0.0894. **B.** circRNAs amplicons obtained from qPCR with Taqman assays on eAAA tissue-derived cDNA. Amplification products from one representative CTRL and one representative eAAA sample are shown in duplicate. **C.** *NFIX, ATM, MYOCD, BMPR2, NRIP1* and *NFATC3* mRNA levels were determined by qRT-PCR and compared in eAAA *vs* CTRL patients. 2^(-ddCT) are plotted. Data are represented as mean ± SEM. Statistics: Unpaired T-test. P values < 0.05 are considered significant. Abbr.: CTRL=control; eAAA: elective AAA.

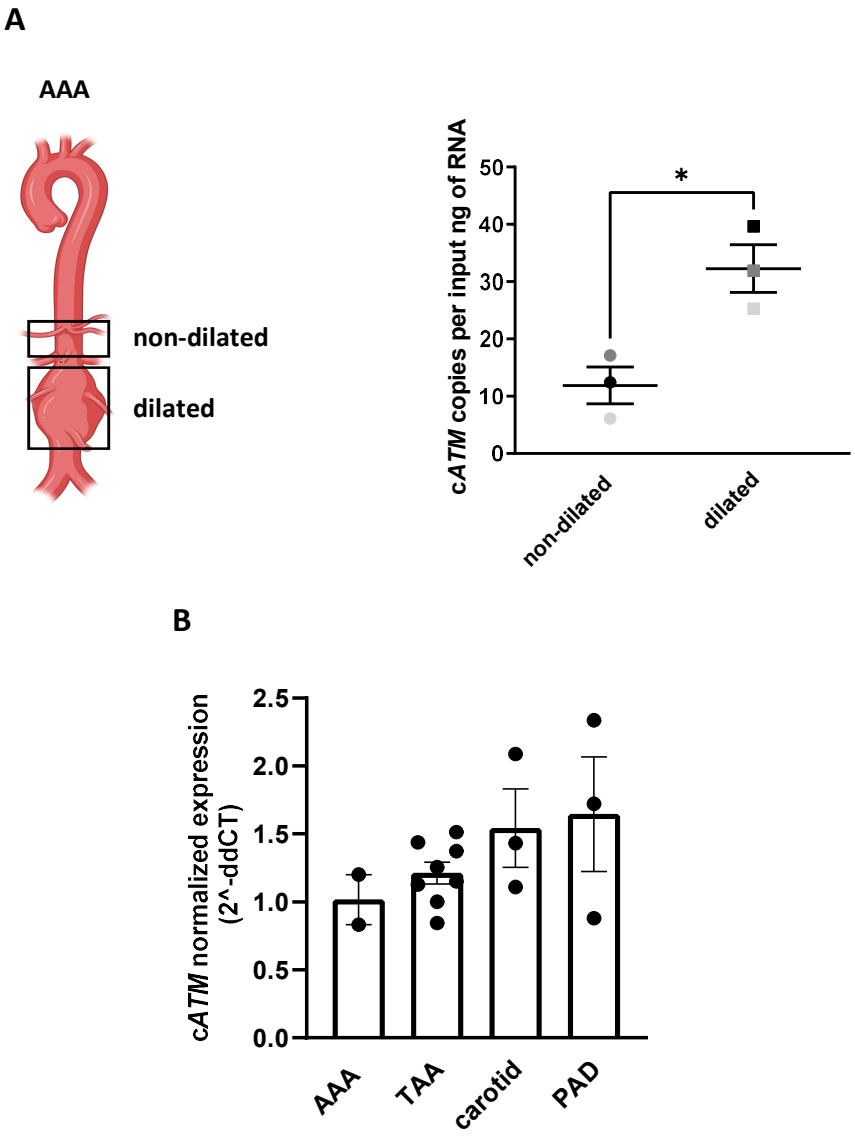

Figure S5. ***Expression of cATM*** **in vascular tissue. A.** *cATM* abundance was quantified by digital PCR in tissue from patients undergoing open repair surgeries, in which both the upstream non-aneurysmal aortic segment (non-dilated control, N=3) and the aneurysmal aortic portion (dilated AAA, N=3) were collected. Different colors indicate different pairs (statistics: paired T-test; P values < 0.05 are considered significant; data are represented as mean ± SEM). **B.** *cATM* expression was assesed by qRT-PCR in different diseased human vascular tissue specimens, including abdominal aortic aneurysm (N=2), thoracic aortic aneurysm (N=8), carotid artery (N=3) and pheripheral artery disease (N=3). Data are represented as mean ± SEM.

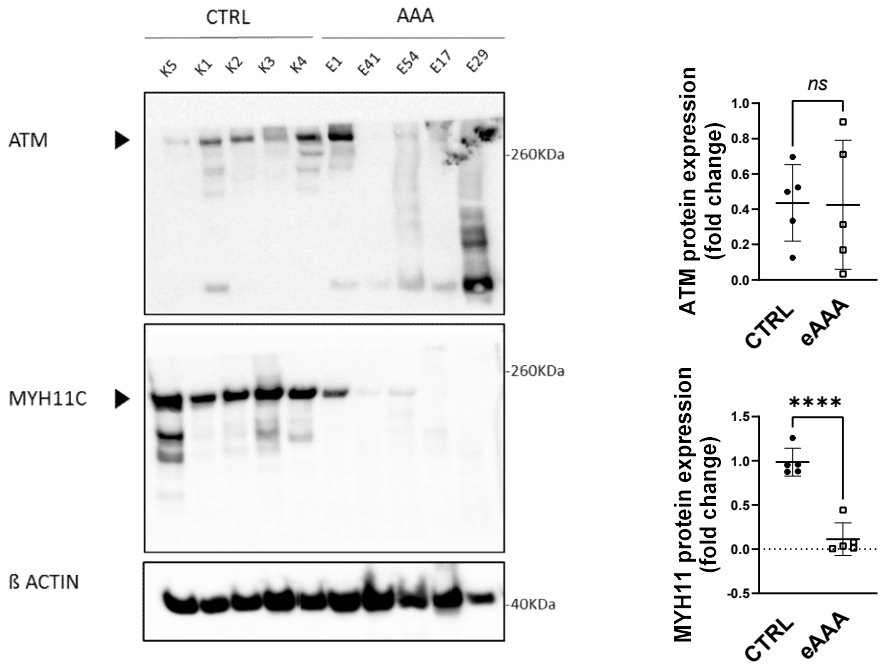

Figure S6. ***ATM protein expression in eAAA vs CTRL patients*****.** WB showing ATM protein in AAA (N=5) vs CTRL (N=5) patients. Black arrows indicate expected molecular weights. Plots on the right show blots quantification (norm.: β actin). Statistics: unpaired T-test; p values < 0.05 are considered significant; data are represented as mean ± SEM. Abbr.: CTRL= control; eAAA: elective AAA.

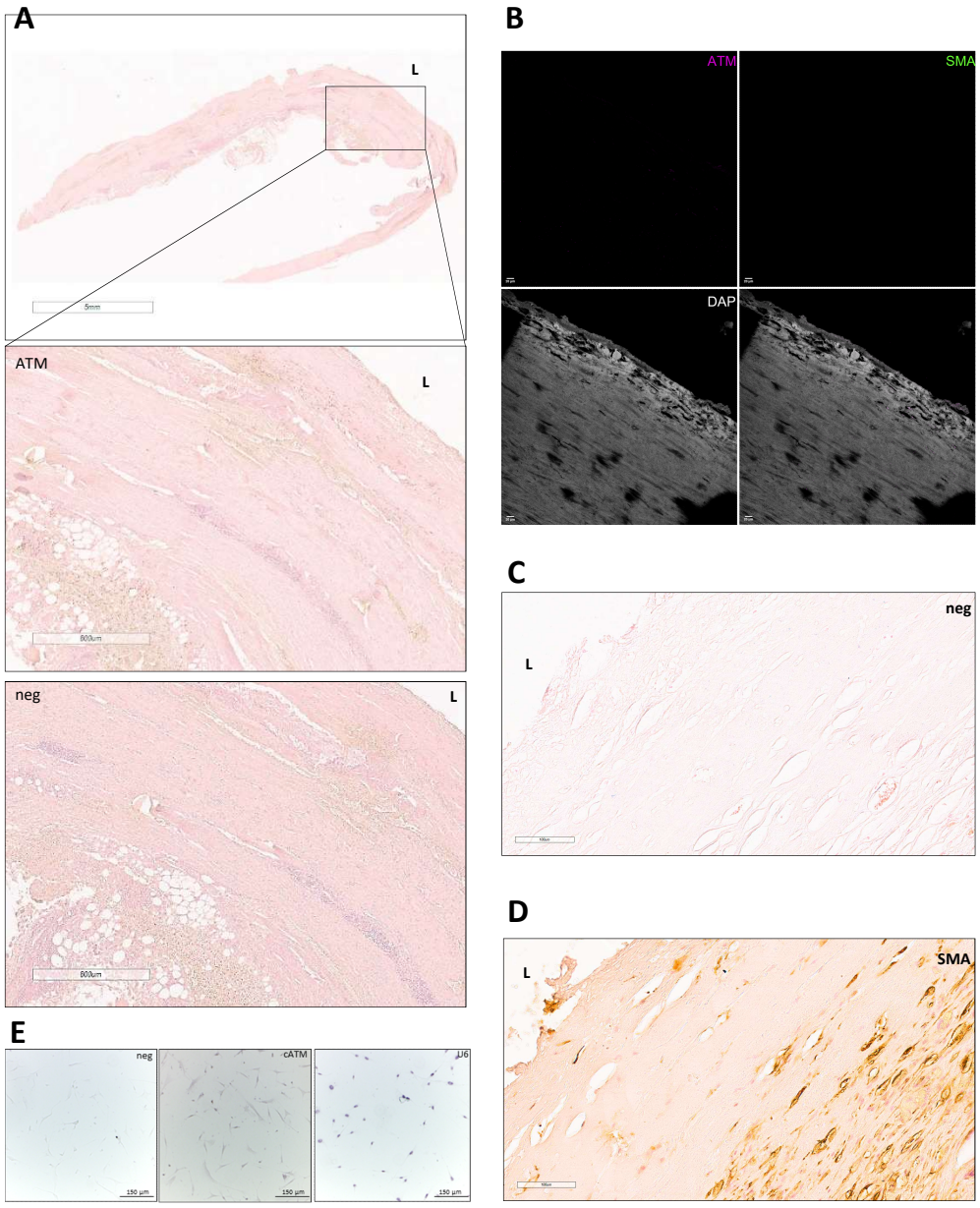

Figure S7. ***ATM protein and cATM staining in human eAAA specimens and AoSMCs.*** **A.** ATM immunohistochemistry in AAA patient section (top) and relative negative control. **B.** ATM and SMA IF negative control. **C.** c*ATM* ISH negative control and (**D**) SMA IHC staining were performed in consecutive slides. **E.** ISH in human aortic SMCs negative control (left), *cATM* (middle) and U6 positive control (right) signal. L= lumen; neg= negative control

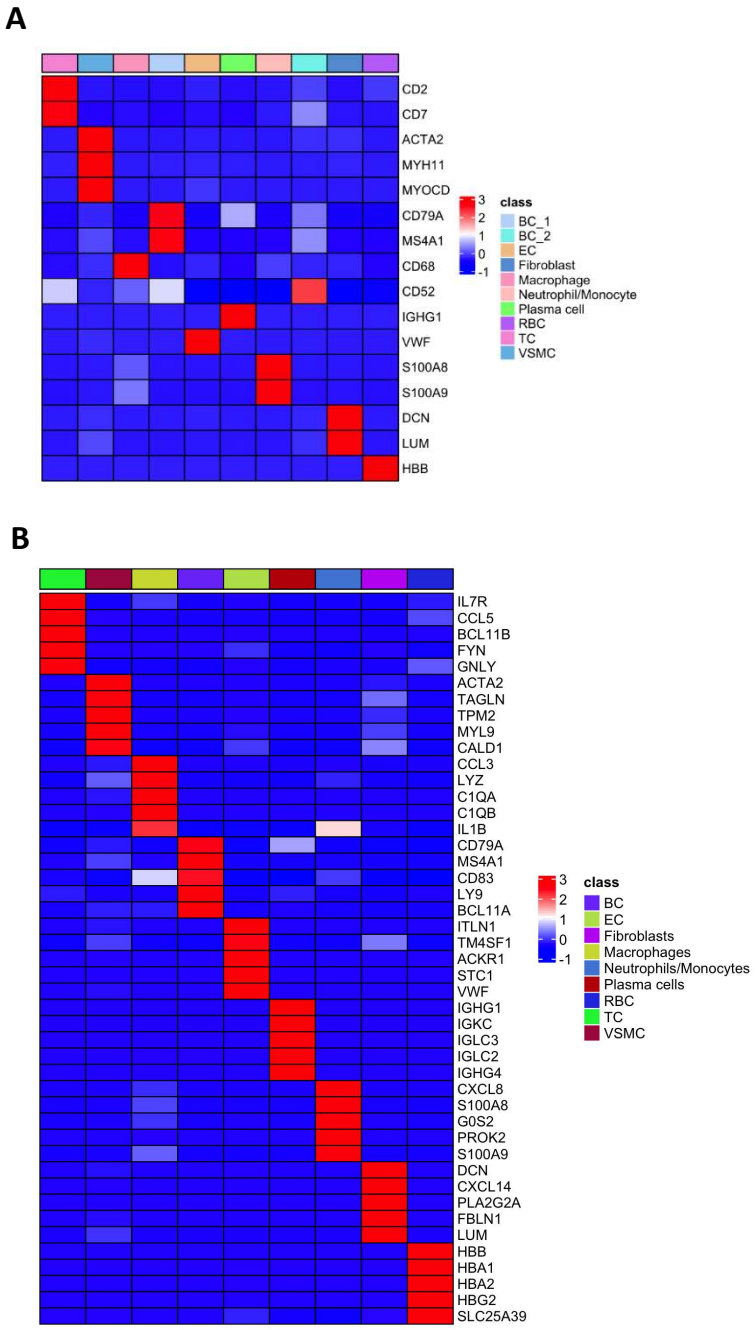

Figure S8. ***Clusters identified by single-cell RNA sequencing of human AAA specimens.*** **A.** Heat maps showing the main gene markers employed for cell clusters labeling and (**B**) summarizing the top five genes for each of the nine identified cell clusters (listed on the right). Color represents the average expression level (blue=low, red= high). Abbr.: BC=B cells; EC=endothelial cells; RBC=red blood cells; TC=T cells; VSMC=vascular smooth muscle cells.

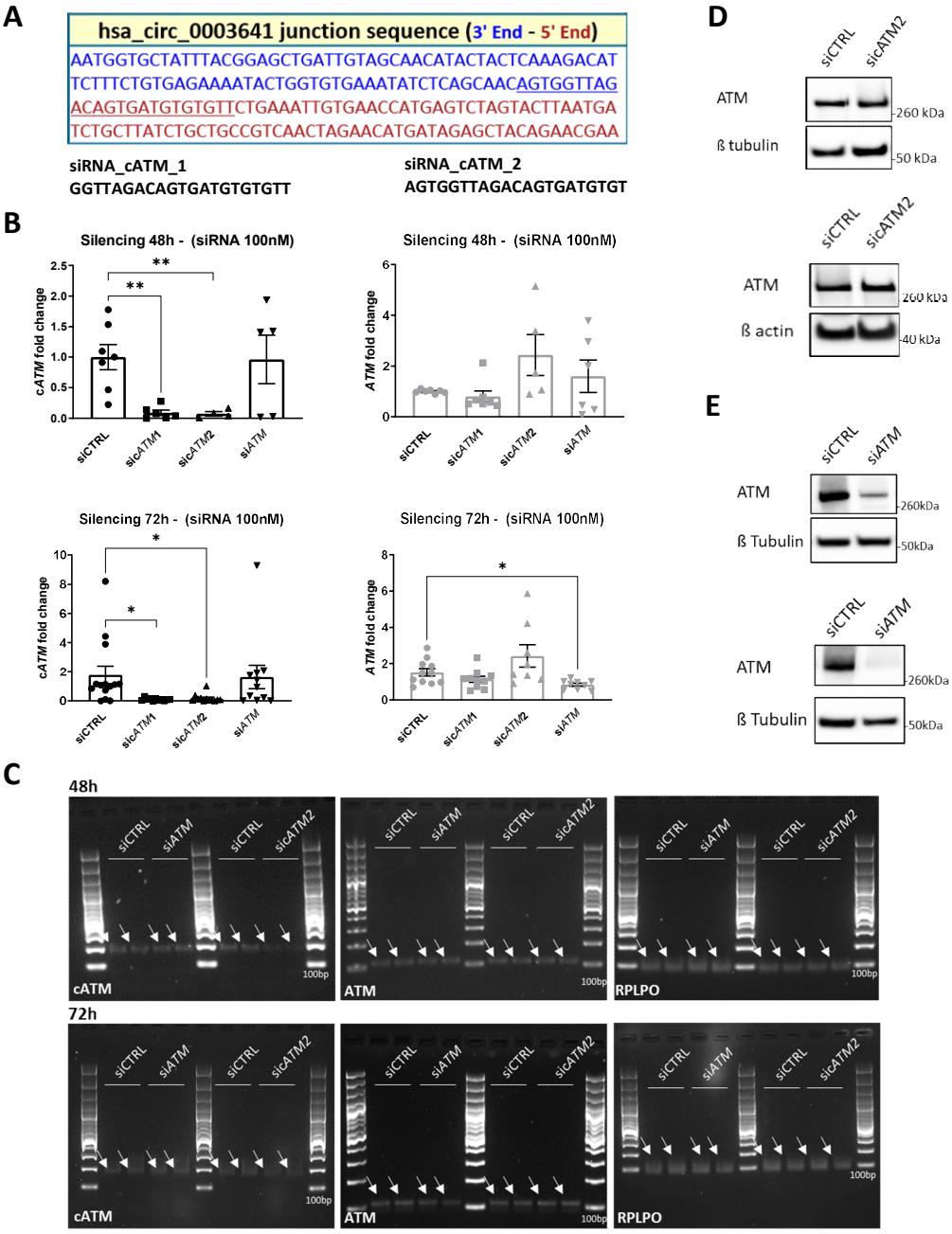

Figure S9. *cATM KD in hAoSMCs*. A. *cATM* (hsa_circ_0003641) siRNA design. The underlined sequence indicates the region covered by two alternative siRNA (si*ATM*1 and si*ATM*2), targeting the backsplicing junction. Different colors indicate different exons. **B** and **C.** qRT-PCR and gel electrophoresis of *cATM*, *ATM* and *RPLPO* amplicons upon c*ATM* or *ATM* KD (100nM siRNA) in control hAoSMCs (statistics: unpaired T-test; p values < 0.05 are considered significant; data are represented as mean ± SEM). **D.** ATM protein levels are not affected by *cATM* KD in both CTRL (top) and AAA-derived AoSMCs (bottom) at 72h, while they are significantly decreased upon *ATM* KD (**E**) in both CTRL (top) and AAA-derived AoSMCs (bottom).

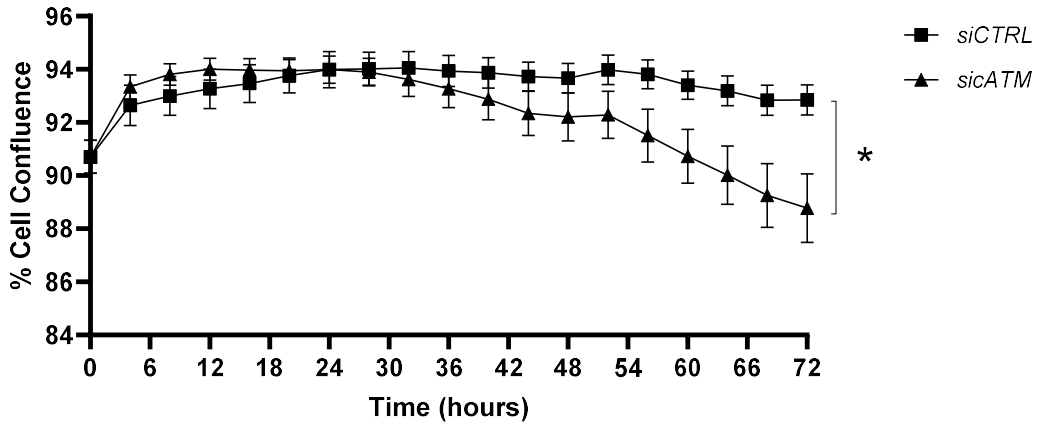

Figure S10. Effects of *cATM KD in hAoSMCs proliferation*. *cATM* was silenced in CTRL AoSMCs and proliferation monitored by live cell imaging. Statistically significant variations in cell confluence were assessed at 72h (statistics: Multiple T-test; p values < 0.05 are considered significant; data are represented as mean ± SD).

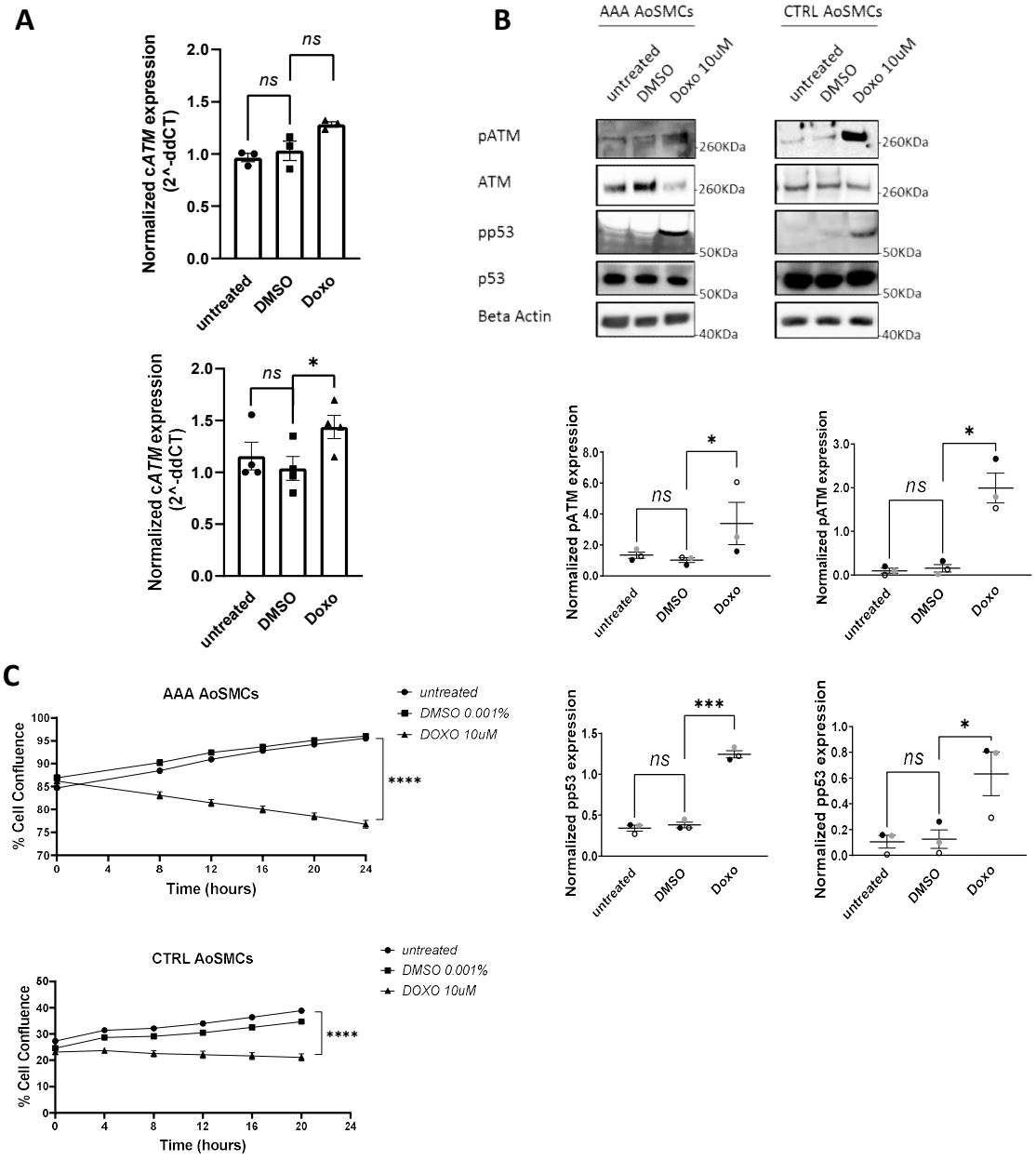

Figure S11. DMSO does not affect c*ATM* expression, phosphorylation of ATM/p53 or proliferation of AoSMCs. A. Expression of *cATM* was assessed after treatment of AAA (top) and CTRL (bottom) AoSMCs with doxorubicin. Administration of 0.001% DMSO did not significantly impact c*ATM* expression, phosphorylation of ATM and p53 (**B,** quantification of blots on bottom-left for AAA and on bottom-right for CTRL AoSMCs) and AoSMCs proliferation dynamics (**C**). (*For panel A:* statistics: Unpaired T-test; p values < 0.05 are considered significant; data are represented as mean ± SEM. *For panel B:* statistics: Paired ratio T-test; p values < 0.05 are considered significant; data are represented as mean ± SEM. For panel C: statistics: Multiple T-test; p values < 0.05 are considered significant; data are represented as mean ± SEM).

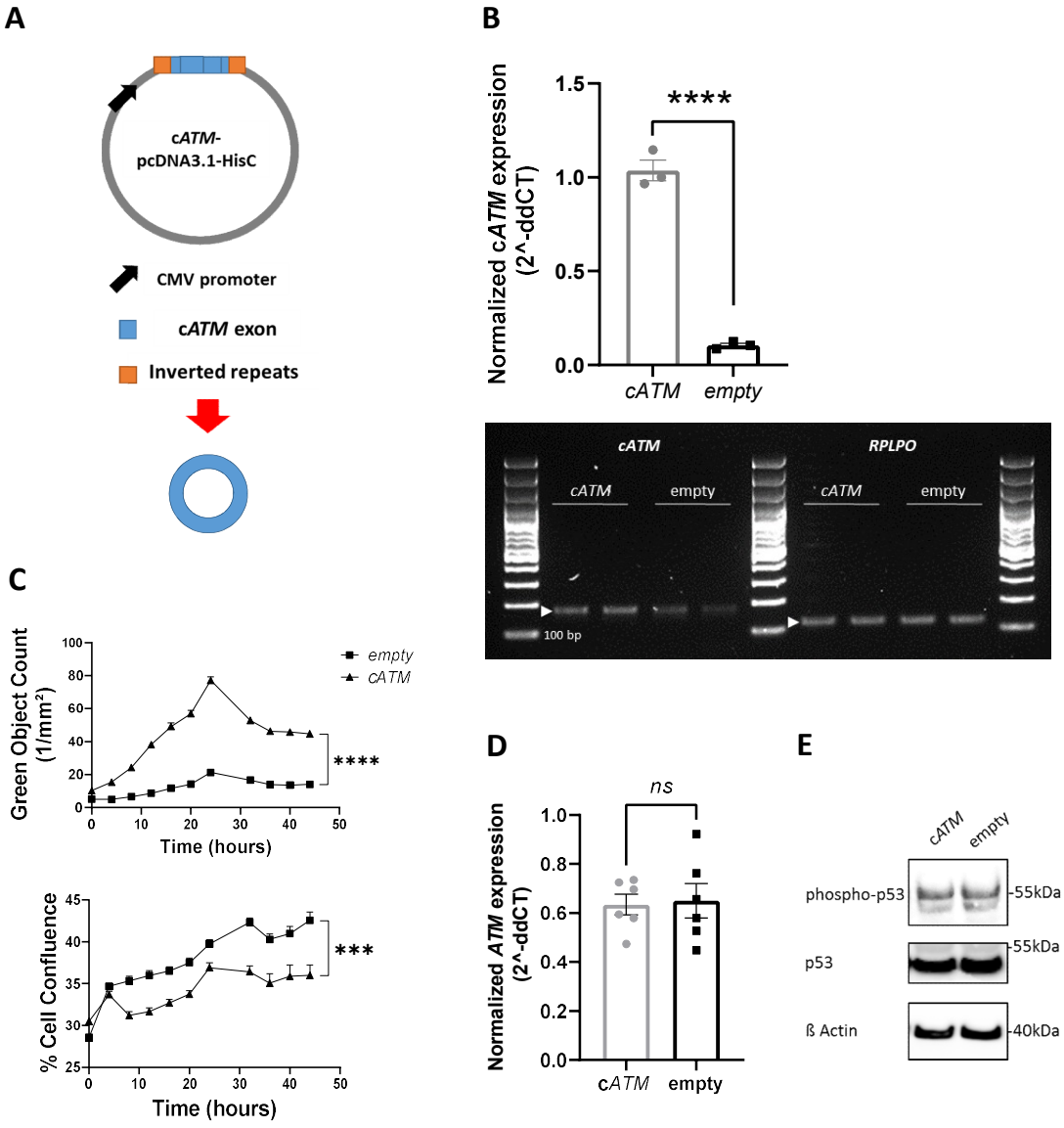

Figure S12. Effects of *cATM overexpression in hAoSMCs*. A. Schematic representation of *cATM* construct. **B.** c*ATM* was overexpressed in CTRL AoSMCs and amplification products obtained from qPCR on cDNA synthesized from transfected cells were run on a gel and sequenced (statistics: unpaired T-test; p values < 0.05 are considered significant; data are represented as mean ± SEM. **C.** Apoptosis and proliferation were monitored by live cell imaging (statistics: Multiple T-test; p values < 0.05 are considered significant; data are represented as mean ± SEM).). **D.** *ATM* mRNA expression and (**E**) phosphorylation of p53 were monitored upon c*ATM* overexpression.

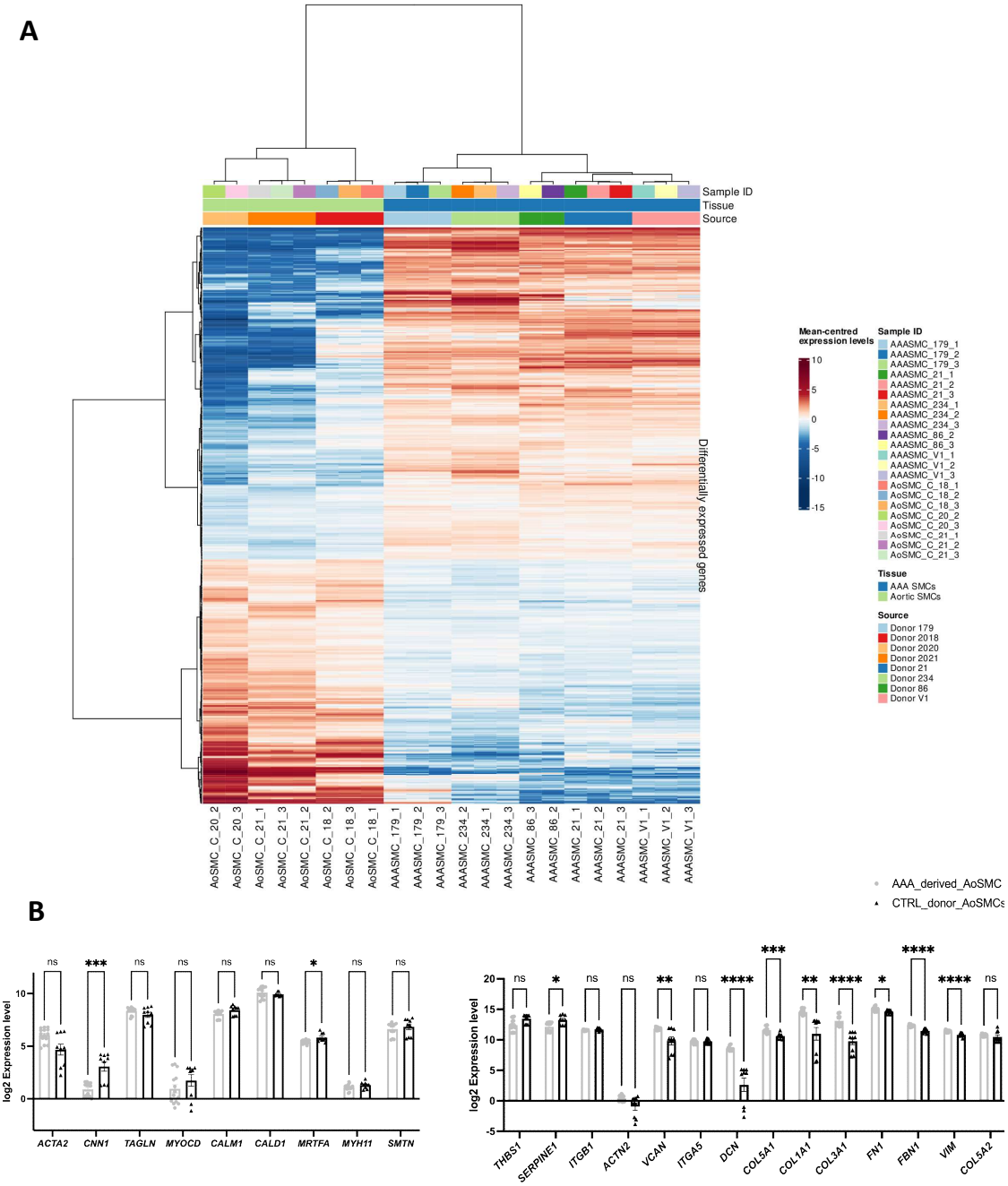

Figure S13. ***Gene expression profile of AAA patient-derived vs control donor AoSMCs.*** **A.** Heatmap showing gene intensity per sample relative to the average level across all samples. Individual genes are shown on the Y axis, while samples are shown along the X axis. Red and blue cells correspond to higher and lower RNAseq levels, respectively. **B.** Differential expression of contractile and synthetic gene markers AAA patient-derived (grey) *vs* control (CTRL) donor (black) AoSMCs. Log2 expression levels are plotted. Statistics: Unpaired multiple T-test. p-values < 0.05 are considered significant. Data are represented as mean ± SEM.

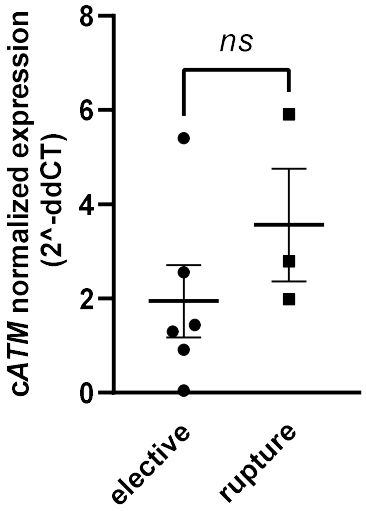

Figure S14. Expression profile of *cATM* in ruptured AAA *vs*. elective patients´ serum samples. *cATM* levels were determined by qRT-PCR in serum samples collected from elective (N=6) *vs* ruptured (N=3) AAA patients. 2^(-ddCT) are plotted. statistics: T-test (two-tailed); p values < 0.05 are considered as significant; data are represented as mean ± SEM.

Figure S15. ***Sanger sequencing of the circular junctions.***

hsa_circ_0003641 (cATM)

AA*TGGTGCTATTTACGGAGCTGATTGTAGCAACATACTACTCAAAGACATTCTTTCTGTGAGAAAATACTG GTGTGAAATATCTCAGCAACAGTGGTTAG*ACAGTGATGTGTGTTCTGAAATTGTGAACCATGAGTCTAGT ACTTAATGATCTGCTTATCTGCTGCCGTCAACTAGAACATGATAGAGCTACAGAACGAA

>PRIMER FWD5

ACACCCTGYTGCCWCTCAAGACTTCTTTCTGTGAGAAATACTGGTGTGAAATATCTCAGCAACAGTGGTT AGACAGTGATGTGTGTTCTGAAATTGTGAACCATGAGTCTAGTACTTAATGATCTGCTTATCTGCTGCCGT AAACTGTSAARCTCCGTTTCATAATTTGTTAATACCMCTATCTCCCCTGTGCTGTTTCCACTGATCTCGCTC CGATWCCTCTTTATGCGTTCTTTTTCGTAKATGAAGTCTGTCTTTTGTTCTGAAMTAATTCWAAA

>PRIMER REV5

GGAAATTGTAGTCCWRAGMTMTGGTTAAATTTMGACACACATCACTGTCTAACCACTGTTGCTGAGAT ATTTCACACCAGTATTTTCTCACAGAAAGAATGTCTTTGAGTAGTATGTTGCTACAATCAGCTCCGTAAAT AGCACCAAATCTGTGCTTTTTCTGTGGGGTTTCKGGTGWAWWWCRCMGSAGGGTTTCGAAAGATCGC GCTGACCCCCCTTTGTGGTCCCTGTGCGTAAA

hsa_circ_0005660 (cNFIX)

*CACCCSGACGTGAGGMGCAGTGCCTCGATGACGGGTGGAACTCATCCCGG*AGTGTGGACACCCATAATC ACTCACAACCTACTATATTCTCTCCTTGTCTGCCCACACTTGTCACAACAGGGACGTGTGTGAC

> PRIMER REV14

AMASAAMYTGGAATCTTTATCTGGCTTACTTTGTCCACACTCCGGGATGAGTTCCACCCGTTCATCGAGG CACTGCTGCCTCACGTCCGCGCTTTCTCCTACACCTGGTTCAACCTGCAACCCTGGAACATCTCAGGAGCT GTGCTGGCCCACAKGCCWGTGTCGTTCTCCTTGTCTGCCGGCCACTTGTAGATAAACATGGACGTGTGT GAASAACCAGCGTCCAGGACGATGCCATACTGSGGGGGAGGGGGAGGSAGWCG

> PRIMER FWD14

CACCCSGACGTGAGGMGCAGTGCCTCGATGACGGGTGGAACTCATCCCGGAGTGTGGACAAAGTAAGC CAGATAAAGATCCAGTTCTTTGATTGTGACTCCAATGTGATGTGGCTAAACTCCCATAATCACTCACAACC TACTATATTCTCTCCTTGTCTGCCCACACTTGTCACAACAGGGACGTGTGTGAC

hsa_circ_0003218 (cBMPR2)

*TCAATTCAGAATGGAACATACCGTTTCTGCTGTTGTAGCACAGATTTATGTAATGTCAACTTTACTGAGAA TTTTCCACCTCCTGACACAACACCACTCA*CTTCGCAGAATCAAGAACGGCTATGTGCGTTTAAAGATCCGT ATCAGCAAGACCTTGGGATAGGTGAGAGTAGAATCTCTCATGAAAATGGGACAATATT

>PRIMER FWD7

ATMMATGAATACCWCCCCCTTYACGTWTRCTGAGATTTTCCACCTCCTGACACAACACCACTCACTTCGC
AGAATCAAGAACGGCTATGTGCGTTTAAAGATCCGTATCAGCAAGACCTTGGGATAGGA

>PRIMER REV7

AAMCWWWKRRMYKTTTSWGMMTAGCCGTTCTTGATTCTGCGAAGTGAGTGGTGTTGTGTCAGGAGG
TGGAAAATTCTCAGTAAAGTTGACATTAMATAAATCTGTGCTACAACAGCAGAAACGGAATCYTTCCCW
AATAAAACTATGTATTTTTTTACCTGTCTCGTAAMATGRCCCATCCCATTGKAAAATTATTGTTTCTTGGTA
CCATTAAACCSWAYGGAAWCCATGCACGACCYTCCGAA

hsa_circ_0042103 (cMYOCD)

*GATGATCTCAATGAAAAAATTGCTCTACGACCAGGGCCACTGGAGCTGGTGGAAAAAAACATTCTTCCTG
TGGATTCTGCTGTGAAAGAGGCCATAAAAG*TTTTACAGTTAAGACTTCAACAAAGAAGGACCCAGGAAC
AACTGGCTAACCAAGGCATAATACCACCACTGAAACGTCCAGCTGAATTCCATGAGCAAAG

> PRIMER FWD9

AGCCCCCGCGTTRMTTWYYTGTTTACKYTAAGACTTCACAMKAAKGACCYMKGAACAACTGGCTAACCA
AGGCATAATACCACACTAATCCAAGCTACAGCAGCCACATACTTACTGCAAAACCTTGCACTGAAACGTC
CAGCTGAATTCCCCSGGTTACCTTCGTTCGTTAGGTTGGACGCGCATCMCATGCAATAGAGGTGGTGTTT
AACTTGYTATAGCTCTGATGTCYGTTCTTYGYACCTTTGTCCGAAGAGGGTWTGTTWTTTTTTTTCATTTW
ACTARTGCKTATTTTTACGGAAACGCWTTGTTTCACCGAAT

> PRIMER REV9

ACCCCCCGWTGATTAAACTGTKTCTCGTGGCWGCTGTCCTTGTCTCACTGTGRTATTATGCCTTGGTTAG
CCAGTTGTTCCTGGGTCCTTCTTTGTTGAAGTCTTAACTGTAAAACTTTTATGGCCTCTTTAACAGCAGAAT
CCACAGGAAATSAMCTCGTTGGGCAATTTGTTGAAGGGCKTCATATTCKCCCWAAGTGKGGGGACGGA
AGCTCTAGCGCTYACSTCGCTTTCTAMATCRATGCTCASAAAAGAAGACCCTCCACTTTTTTMTTTGACCT
ATGCCKATATTGAACGARATGWTTATCTCCCCGACTCCGATCCCTCCTCATGGATTACYACRGCTCMATW
TCGAWC

hsa_circ_0004771 (cNRIP1)

*CAGGGAATCTGAAGACTCCGGATGACATCAGAGCTACTTTTCAACAGCCTTCTCAATTTTCTTTCTCAGAA
AGCAGAGGCTCAGAGCTTGGAGACAGACG*GAAGTGTTTGGATTGTGAGCTATTTCAGAACTGTTCTCAG
GACTCATTATTTTAACATTTGGGAGAAACACAGCCAGAAGATGCACACTTGACTGAAGGA

PRIMER FWD2_HW

CCCCTTCTTCCAATTTTCTTTCTCAGAAAGCAGAGGCTCAGAGCTTGGAGACAGACGGAAGTGTTTGGAT
TGTGAGCTATTTCAGAACTGTTCTCAGGACTCATTATTTTAACATTTGGGAGAAACACAGCCAGAAGATG
CACAAA

PRIMER REV2_HW

TCCCMKTTAAAATTGAGTCCTGAKAACAGTTCTGAAATAGCTCACAATCCAAACACTTCCGTCTGTCTCCA
AGCTCTGAGCCTCWGCTTTCTGAGAAAGAAAATTGAGAAGGCTGTTGAAAAGTAGCTCTGAGGTCATCC
GGA

hsa_circ_0005615 (cNFATC3)

*AGTATCCTTTAAAGAAAGATTCATGTGGTGATCAGTTTCTTTCAGTTCCTTCACCCTTTACCTGGAGCAAAC
CAAAGCCTGGCCACACCCCTATATTTCG*ATCTTGAGCCAGATGATTGTGCATCCATTTACATCTTTAATGTA
GATCCACCTCCATCTACTTTAACCACACCACTTTGCTTACCACATCATGGATTACC

PRIMER FWD5_HW

TCCAACGGCACCCKATATTTCGATCTTGAGCCAGATGATTGTGCATCCATTTACATCTTTAATGTAGAKCC
ACCTCCATCTACTTTAACCACACCACCTTTGCTTACCAAG

PRIMER REV5_HW

TAAARTGGAGTGGAWCTACATTAAAGATGTAAATGGGATGCACAATCATCTGGCTCAAGATCGAAATAT
AGGGGTGTGGCCAGGCTTTGGTTTGCTCCAGGTAAAGGGTGACT

DOWNSTREAM EXON

UPSTREAM EXON

VALIDATED SEQUENCE (SANGER)

Figure S16. ***cATM-pcDNA3.1-HisC - 2669bp.***

LINE repeat
MLLT3/AF9 intron 4 (chr9:20414651+20415428
ATM intron
Simple repeat
ATM exons
Splicing sites
EcoRI
XhoI

GAGCGCGACGTAATACGACTCACTATAGGGCGAATTGAGTGAAGGCCGTCAAGGCCGCATGAATTCTTTCTTAATC
ATCTGAAGCATGGAGTTTTAAAACATTTCAATTCAACAAATGTTAACTACTGCTTGTCCTAGAAGATACAAGGATGA
ATAACACATGGACCCCACCCTTAATAACTATGACGTATCTATGATTGATAGATGTTGACAACCAAAAGACGGGAAC
TATTAATTCTGTTGGGAGCATGGGGCGAAGAATAATTCAAAAATTCATAAAGAAGTAACATCTGAATTAGGTCCTG
GAGGATAAACAGGTAGTTACTAGAATGAAAAGAATGGAAAGGTACTTAAGAGACCAAGGACCAGAATAAACTAA
AACAACAGGGAGCAAAGCACAGATTGTATTTGGGGAACACCCAGCTATAGAACAAGATTGAGAAGGAGGCAGAA
AAATAGCCCAGCTTCACATAGTAAGGTCAGATTACATTAAATTTCAAATGGCTTTGCAATATAAGGAATCATAAAAC
CCCCCCAAAAGAAATAAAGTAATTCTCAATTTGAGATAAAAAGCAATTATTTTTATGCTGTATAAAATTTCATCAGTT
AAGAACTGTATCTCTCACCCACTAGGAAAAATAAAAGGAAGTTAATAGAACAAAGATTTCACCTAACCATCAAATG
GACTAGAAAGTCTTTAGCAATTACTGTATTTTGATCATGAGAAAAGACGTAATTGCTGCCTATTTCATTTTAAATATG
ATCAATTTTTCCACTCATATAAACATATCAGAATATATAACCTATATATAATCTTTCTGTTTAGGAACAAAATCTAAGT
CCAGATATCCAGATTACTTGTATAGATTTTAAGAAAATCTCATTTTAAATACGGAAATGTTAAGAAAAATTATTGTG
CCTTTGACCAGAATGTGCCTCTAATTGTACAGTTAAATCTAACTATAAATACTGCAGTATAAAATAATTATATACACA
TTTTTTCACACCTCTTTCTCTCTATATATGCATATATACATATACATATATATACCTATATGTATTTTTTTTACAGACAG
TGATGTGTGTTCTGAAATTGTGAACCATGAGTCTAGTACTTAATGATCTGCTTATCTGCTGCCGTCAACTAGAACAT
GATAGAGCTACAGAACGAAAGAAAGAAGTTGAGAAATTTAAGCGCCTGATTCGAGATCCTGAAACAATTAAACAT
CTAGATCGGCATTCAGATTCCAAACAAGGAAAATATTTGAATTGGGATGCTGTTTTTAGATTTTTACAGAAATATAT
TCAGAAAGAAACAGAATGTCTGAGAATAGCAAAACCAAATGTATCAGCCTCAACACAAGCCTCCAGGCAGAAAAA
GATGCAGGAAATCAGTAGTTTGGTCAAATACTTCATCAAATGTGCAAACAGAAGAGCACCTAGGCTAAAATGTCAA
GAACTCTTAAATTATATCATGGATACAGTGAAAGATTCATCTAATGGTGCTATTTACGGAGCTGATTGTAGCA*ACAT*
ACTACTCAAAGACATTCTTTCTGTGAGAAAATACTGGTGT**GAAATATCTCAGCAACAGTGGTTAG**GTATGTTTTGA
AGGTTGTTGTTTGTGAATTTTTCCTCATGAAATGAAACTTCACCAAAGAAAGCACTCTGTCTGTATCTGTCTATATCC
CCCAAGTGACCTGACAGTTTAACAGTACTTTAGTAAAATTATATGGTTATCGAACTGACCCTTAATTTTTATTTATTA
TGTAGCTTTTGAATAAAGTCATGAATAATATATCAGGTGCCTGATATCAGAGCCGATATCTGGACTTAGATTTTGTT
CCTAAACAGAAAGATTATATATAGGTTATATATTCTGATATGTTTATATGAGTGGAAAAATTGATCATATTTAAAAT
GAAATAGGCAGCAATTACGTCTTTTCTCATGATCAAAATACAGTAATTGCTAAAGACTTTCTAGTCCATTTGATGGT
TAGGTGAAATCTTTGTTCTATTAACTTCCTTTTATTTTTCCTAGTGGGTGAGAGATACAGTTCTTAACTGATGAAATT
TTATACAGCATAAAAATAATTGCTTTTTATCTCAAATTGAGAATTACTTTATTTCTTTTGGGGGGGTTTTATGATTCCT
TATATTGCAAAGCCATTTGAAATTTAATGTAATCTGACCTTACTATGTGAAGCTGGGCTATTTTTCTGCCTCCTTCTC
AATCTTGTTCTATAGCTGGGTGTTCCCCAAATACAATCTGTGCTTTGCTCCCTGTTGTTTTAGTTTATTCTGGTCCTTG
GTCTCTTAAGTACCTTTCCATTCTTTTCATTCTAGTAACTACCTGTTTATCCTCCAGGACCTAATTCAGATGTTACTTCT
TTATGAATTTTTGAATTATTCTTCGCCCCATGCTCCCAACAGAATTAATAGTTCCCGTCTTTTGGTTGTCAACATCTAT
CAATCATAGATACGTCATAGTTATTAAGGGTGGGGTCCATGTGTTATTCATCCTTGTATCTTCTAGGACAAGCAGTA
GTTAACATTTGTTGAATTGAAATGTTTTAAAACTCCATGCTTCAGATGATTAAGAAACTCGAGCTGGGCCTCATGGG
CCTTCACTTCACTGCCCGCTTTCCAGTCGGGAAACCTGTCGTGCCA

Figure S17. ***Cloning strategy.***

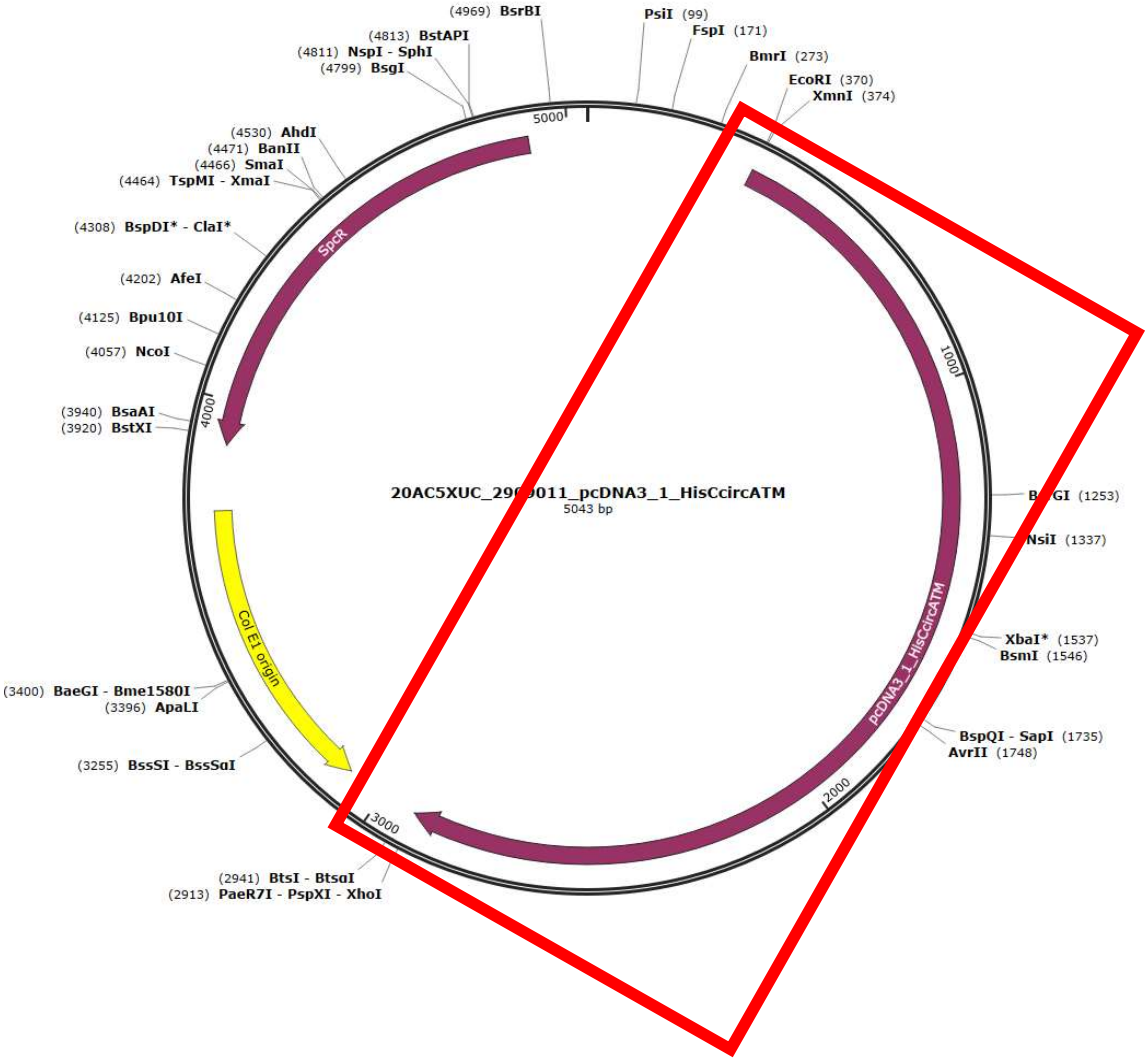

Mammalian expression vector
(Restriction: EcoRI/XhoI in ***pcDNA3.1-HisC****)*

Figure S18. ***qPCR amplicon Sanger sequencing of cATM-pcDNA3.1-HisC-transfected AoSMCs.***

hsa_circ_0003641 junction sequence (3' End - 5' End of circRNA)
AATGGTGCTATTTACGGAGCTGATTGTAGCAACATACTACTCAAAGACATTCTTTCTGTGAGAAAATAC TGGTGTGAAATATCTCAGCAACAGTGGTTAG ACAGTGATGTGTGTTCTGAAATTGTGAACCATGAGTCT AGTACTTAATGATCTGCTTATCTGCTGCCGTCAACTAGAACATGATAGAGCTACAGAACGAA

in grey: SANGER VALIDATED

>cATM_c30 B1+cATM_fwd

NHNWNTCAAGANMMNTTCTTTCTGTGNNAAATACTGGNTGTGAAATATCTCAGCAACAGTGGTTAGACAGTNM YGNN

>cATM_c30 B1+cATM_rev

NNTTTNNGANCACACATCACTGTCTAACCACTGTTGCTGAGATATTTCACACCAGTATTTTCTCACAGAAAGAATGT CTTTGAGTAGTATGTTGCTACAATCAGCTCCGTAAATAGCACCNNNNM

>cATM_c30 B2+cATM_fwd

NAAGANTTCTTTCTGTGAGAAATACTGGTGTGAAATATCTCAGCAACAGTGGTTAGACAGTGATGTGTGTTCTGAA ATTGTGAACCATGAGTCTAGTACTTAATGATCTGCTTATCTGCTGCCGTN

>cATM_c30 B2+cATM_rev

NNAATTTCNGAACACACATCACTGTCTAACCACTGTTGCTGAGATATTTCACACCAGTATTTTCTCACAGAAAGAAT GTCTTTGAGTAGTATGTTGCTACAATCAGCTCCGTAAATAGCACCAAANCNT